M 2015

U.PORTO

FEUP FACULDADE DE ENGENHARIA
UNIVERSIDADE DO PORTO

POLY(ETHYLENE TEREPHTHALATE): MODIFICATION AND CHARACTERIZATION AIMING TENDON REPAIR

ANA FILIPA PAULOS FERREIRA BRANDÃO

DISSERTAÇÃO DE MESTRADO APRESENTADA

À FACULDADE DE ENGENHARIA DA UNIVERSIDADE DO PORTO EM

MIEMM – MESTRADO INTEGRADO EM ENGENHARIA METALÚRGICA E DE MATERIAIS

ORIENTADORA: PROF.ª DOUTORA MARIA ASCENSÃO FERREIRA SILVA LOPES

CANDIDATO	Ana Filipa Paulos Ferreira Brandão	*Código*	201006593
TÍTULO	Poly(ethylene terepgthalate): modification and characterization aiming tendon repair		
DATA	27 de julho de 2015		
LOCAL	Faculdade de Engenharia da Universidade do Porto – Sala F106 - 11:00h		

JÚRI	*Presidente*	Professor Doutor Fernando Jorge Mendes Monteiro	DEMM/FEUP
	Arguente	Professor Doutor Rui Jorge Sousa Costa de Miranda Guedes	DEMec/FEUP
	Orientador	Professora Doutora Maria Ascensão Lopes	DEMM/FEUP

ABSTRACT

Tendon injuries affect both young and old population worldwide. When a tendon injury occurs, it healing mechanism is inefficient. Therefore, since current treatments available have limited success, it is important to use scaffolds that can enhance tendon tissue regeneration and, at the same time have the adequate mechanical properties. The present work aims to optimize a poly(ethylene terephthalate)(PET) surface functionalization in order to enhance cell-material interaction during tendon tissue regeneration. In the future, the developed grafting approaches can be extrapolated to the PET textile structures under development for tendon repair. These structures were also characterized in order to select the best structure to be use in the final tendon scaffold. The PET yarn characterization indicated that its crystallinity degree was about 55%, that it was able to absorb water and that, up to 1 month test, degradation did not occur. Moreover, the braided structure that revealed to be more suitable to fulfill the tendon scaffold requirements was the 16 yarn braid one, produced with the highest take-up rate because presented the highest capillary rise and mechanical properties, such as maximum force and stiffness. For the PET functionalization, the initial oxygen plasma treatment was able to low the polymer water contact angle from 74.7 ° to 10.7 °, enhancing wettability. After plasma treatment, two grafting approaches were performed, with ethylenediamine and D-Lysine and from each one it was selected the condition that presented to have more potential to cell culture in vitro testing. The ethylenediamine based condition selected (W5050) presented the highest amino group density and wettability, whereas the selected D-Lysine based condition (pH 9.5) was the one that demonstrated to have a thicker coating and higher wettability than untreated PET. From the evaluation of cells viability on the grafted samples, it was observed a high cell response on all grafted samples compared to untreated PET, showing the ethylenediamine grafting more cellular metabolic activity as supported by scanning electron microscopy that showed a cell morphology and growth that indicated good cell adhesion to the functionalized material have occured.

Key Words: Tendon tissue engineering, PET surface functionalization, tendon repair

RESUMO

As lesões do tendão afetam, a nível mundial, não só a população mais idosa mas também a mais jovem. Quando uma lesão ocorre, o seu mecanismo de regeneração não é eficiente. Por isso, uma vez que os tratamentos atuais têm um sucesso limitado, é importante utilizar *scaffolds* que sejam capazes de melhorar a regeneração do tecido do tendão e que, ao mesmo tempo, tenha as propriedades mecânicas adequadas. O presente estudo tem como objetivo otimizar uma modificação da superfície de poli(etileno tereftalato) (PET), de modo a melhorar a interação entre célula-material durante a regeneração do tendão. Futuramente, as abordagens selecionadas poderão ser extrapoladas para estruturas têxteis de poli(etileno tereftalato) que estão a ser desenvolvidas para regeneração do tendão. Estas estruturas foram também caracterizadas com o objetivo de selecionar a melhor estrutura a ser usada num *scaffold* para regeneração do tendão. A caracterização do fio de poli(etileno tereftalato) indicou que a sua cristalinidade é de aproximadamente 55%, que este é capaz de absorver água e que, até 1 mês de ensaio, não ocorre degradação. Para além disso, o entrançado que revelou ser mais adequado para cumprir os requisitos impostos a um *scaffold* para tendões foi a estrutura com 16 fios produzida com uma velocidade de saída superior, porque apresentou maior capilaridade e propriedades mecânicas, como força máxima e rigidez. Quanto à modificação do poli(etileno tereftalato), o tratamento inicial de plasma com oxigénio foi capaz de diminuir o ângulo de contacto do polímero de 74,7 ° para 10,7 °, melhorando a molhabilidade. Após o tratamento por plasma, duas abordagens de funcionalização foram realizadas, com etilenodiamina e D-Lisina e, de cada, foi selecionada a condição que apresentou maior potencial para ser testada com culturas celulares *in vitro*. A condição de etilenodiamina selecionada (W5050) apresentou elevada densidade de grupos amina e molhabilidade, e a condição seleccionada da D-Lisina (pH 9,5) foi a que demonstrou ter o revestimento mais espesso emaior molhabilidade do que a amostra de poli(etileno tereftalato) não tratada. O estudo da viabilidade das células no PET mostrou uma maior reposta celular em todas as abordagens de funcionalização em relação ao PET não modificado, apresentado a etilenodiamina maior atividade metabólica, o que foi confirmado com as imagens de microscopia eletrónica de varrimento que mostraram um crescimento celular e morfologia que indica que ocorreu uma boa adesão celular no material.

Palavras-chave: Engenharia de tecidos do tendão, modificação da superfície de PET, regeneração do tendão

Aknowledgments

CONTENTS

LIST OF TABLES

ABBREVIATIONS AND SYMBOLS

List of abbreviations:

AFM	Atomic Force Microscopy
DSC	Differential scanning calorimetry
ECM	Extracellular matrix
EDA	Ethylenediamine
FTIR-ATR	Fourier transform infrared attenuated total reflectance spectroscopy
PBS	Phosphate buffered saline
PET	Poly(ethylene terephthalate)
SEM	Scanning eletron microscopy
XRD	X-Ray diffraction

List of symbols:

θ	Contact angle

CHAPTER 1 - INTRODUCTION

1.1. MOTIFS AND OBJECTIVE

Nowadays, tendon and ligament injuries represent an import aspect to consider both in sports and working activities. These kind of injuries are frequent and affect not only the older population but also younger people. They are caused by the incomplete healing of the tendon injury, ranging from strains to complete rupture and affect mainly the adult population [1-3].

Literature reports that, in Finland, a population of 5 million has more the 200 000 acute sports-related injuries per year and, in the USA, it is estimated that 30% to 50% of overuse injuries are related with the practicing of sports. In fact, in the USA 51% of people over 80 years experienced rotator cuff injury, with over 50,000 patients requiring surgical repair and 11% of regular runners suffer from Achilles tendinopathy. Thus, represents a significant treatment cost to the healthcare system of each country; for instance, in the USA the total costs for tendon and ligament injury has been estimated at $30 billion annually [1-5]

Because of the market demand, biomaterials have become critical components in the development of effective new treatments. For over 15 years, tissue engineering has been developing scaffolds for tendon regeneration. Scaffolds may be biological and synthetic, although biological ones have higher biocompatibility, they present lower mechanical properties, when compared with the synthetic ones. The main issue nowadays is to produce scaffolds that mimic the tendon tissue [2, 5].

This master dissertation is related with tendon repair and is inserted on Diana Morais PhD work that is developing a tendon scaffold structure, based on textile technology, aiming to achieve the minimum requirements in terms of mechanical properties. The main objective of this master dissertation is to functionalize one of the polymer being used on Diana Morais structures, that in this case is poly(ethylene terephthalate), in order to increase its response to biological tissues when applied in tendon tissue regeneration. Moreover, the poly(ethylene terephtalate) structures being developed are also going to be characterized in terms of physico-chemical and mechanical properties.

1.2. TENDON STRUCTURE AND FUNCTION

Tendons are dense fibrous connective tissue that physically connects the muscle to bone and allow transmission of forces, resulting in locomotion and joint stability. Also, due to numerous extracellular fibers arranged in regular arrays, it is classified as dense regular connective tissue **[6-8]**.

The tendon possesses a multi-unit hierarchical structure consisting of collagen molecules, fibrils, fiber bundles, fascicles and tendon units. This tissue is characterized by the presence of an abundant extracellular matrix (ECM), mainly composed of collagen I, resulting on a hypocellular structure. Although this type of structure, tenoblasts and tenocytes constitute about 90% to 95% of the cellular elements of tendons; while tenoblasts are immature cells, with high metabolic activity, tenocytes are mature tenoblasts with decreased metabolic activity **[1, 6, 7, 9]**.

The extracellular matrix is mainly composed by type I collagen (30% of tendon dry weight), elastin (2% of tendon dry weight) and ground substance (68% of tendon dry weight) **[4, 6]**.

About type I collagen, its molecules can self-assemble into highly organized fibrils, which are cross-linked, conferring them a high tensile strength which, on the other hand, provides mechanical strength to the tendon tissue. In addition, collagen fibrils exhibit a crimped, waveform appearance, in the rested state, which plays an important role in its mechanical properties. For instance, the crimped pattern explains tendons nonlinear elastic behavior **[3, 4, 10]**.

The angle and length of the crimp depends on the tendon features; when it has a small angle, its fibers have a mechanically weaker structure. In addition, crimp acts as a shock absorber along the length of the tissue and also provides a buffer in which slight longitudinal elongation can occur without fibrous damage **[4, 10]**.

Elastin is important because it contributes to the flexibility of the tendon because it helps the collagen fibers to recover their wavy configuration after muscle contraction and tendon stretch **[4, 11]**.

Lastly, ground substance has a high viscosity that provides the structural support, lubrication and spacing of the fibers, allowing their gliding. Moreover it

allows the diffusion of nutrients and gases and regulates the extracellular assembly of procollagen into mature collagen **[4]**.

Once ground substance is composed by various molecules, they confer different properties such as rapid diffusion of water-soluble molecules and migration of cells and mechanical stability; moreover, some molecules may act as a template for collagen fiber formation, playing an important role in collagen fiber alignment and orientation **[6, 11]**.

1.3. MECHANICAL PROPERTIES OF TENDONS

The mechanical properties of tendons are very complex due to their structure; their primary role is to transmit tensile forces from the muscle to bone and act as a buffer by absorbing external forces to avoid muscle damage. To perform their role, tendons exhibit high mechanical strength, good flexibility and an optimal level of elasticity **[4, 12, 13]**.

The functional mechanical behavior of a tendon, in the normal anatomical setting, depends upon several factors that may affect the force-elongation curve. Larger tendons can resist more force, longer tendons can elongate further under the same load; a higher proportion of type I collagen, or larger collagen fibers, create a stronger tendon; and increased crosslinking indicates a stiffer tendon that will deform less under the same loading conditions **[4]**.

The mechanical behaviour of collagen is dependent on the number and types of intra- and inter-molecular bonds. A typical stress-strain curve of an isolated tendon helps to demonstrate the behaviour of the tendon in elongation-to-failure conditions and it can be identified 3 distinctive regions, as can be seen in figure 1 **[4, 12, 14]**.
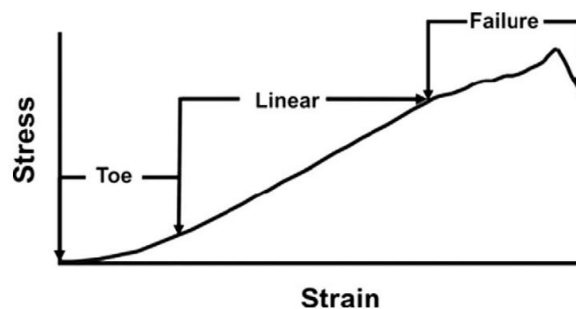
Figure 1 – Stress-strain curve of a normal tendon [14].

The initial concave portion of the curve is the first region, named *toe region*, where the stiffness (curve slope) is gradually increased and the tendon is strained up to 2% **[4, 12]**.

So, loads within this region will elongate tendons by reducing the crimp angle, however these loads do not cause further fiber stretching. Therefore, in this region the tendon elastic limit is not exceed and, subsequent unloading restores the tendon initial length and crimped configuration; these phenomenon may be explained by the presence of elastin fibers, that are responsible for bringing the stretched collagen bundles back to the resting state **[4, 12, 14]**.

When further elongation is performed, the tendon reaches a second region, named as *linear region*, where the stiffness remains constant and the collagen fibers are no longer crimped; so elongation is due to the stretching imposed to the already aligned fibers. Moreover, at the end point of the *linear region,* unloading does not restore the tendon initial length and some fibers start to fail **[4, 12, 14]**.

Thus, during the different portions of the *linear region*, understanding the physical changes that the tendon suffers may be more important in explaining the tissue damage that occurs during an injury than knowing the maximum load the tendon can tolerate before breaking **[4]**.

If elongation continues beyond the *linear region,* the tendon enters the third region, named as *failure region*, where failure of the collagen fibers occurs in an unpredictable way causing tears in the tendon and, finally, leading to the tissue total rupture **[4, 12, 14]**.

1.4. TENDON INJURIES

An adult tendon has low regenerative capacity, cell density, nutrient and oxygen; even so it suffers some of the highest mechanical loads in the body. When these loads go above a critical point, it may cause permanent tissue damage that results in decreased function and mobility, thus dramatically affects the patient's quality of life **[1, 15].**

Tendon injuries can be acute or chronic and are caused by intrinsic and extrinsic factors, either alone or a combination of both. While acute injuries are mainly due to extrinsic factors, the chronic ones are mainly caused by intrinsic factors.

Intrinsic factors are related with excessive body weight, diseases and aging; extrinsic factors include environmental conditions, prescription drugs, nutrition and lifestyle [1, 7, 12].

Though all the factors cited above, mechanical loading on tendon tissues, mainly on elder people, is the main factor that leads to tendon pathological changes such as tendinopathy. Tendionpathy describes tendons clinical conditions that result from overload and overuse injuries and can be classified as tendinitis or tendinosis [1, 12].

An acute injury is related to tendinitis and it consists in a tendon inflammation that results from micro-tears that occurs when the muscle and the tendon undergo and acute overload with a tensile force that is too heavy or too sudden. On the other hand, tendiosis is associated with a chronic injury, where a non-inflammatory degeneration of tendon's collagen happens in response to chronic overuse; when this overuse is continue, the tendon doesn't have time to heal and rest properly and it leads, eventually, to tendon rupture [1, 4, 16].

The Achilles tendon is the most frequently rupture tendon and, along with the patellar and flexors tendons, they are the most commonly tendons affected by tendinopathies. These tendons are the most frequently injured because they are highly stressed, being expose to repeated strains and have less vascularization [1, 17].

The Achilles tendon is the largest tendon in the body and enables walking, running and jumping but, at the same time, is the most common source of disability in athletes due to continuous and intense functional demands imposed on it. The incidence of Achilles tendon injuries has been rising and often causes severe, persistent pain and disability and it is difficult to repair due to the mechanical demand [1, 4, 17, 18].

The patellar tendiopathy, which is a painful degenerative and chronical condition, constitute a significant problem in a wide variety of sports, being over 30% of sports-related injuries. Finally, flexor tendons injuries are frequently associated with nerve and vascular injuries and required tendon grafting to repair [1, 4, 18].

1.5. TENDON HEALING PROCESS

When the tendon is injured, in order to restore the functions of a normal tendon, it is necessary to reestablish the tendon fibers and the gliding mechanisms between tendon and the surrounding structure. However, this process is slow and inefficient that never fully restores the biological and biomechanical properties **[1, 14]**.

After tendon injury, the process of healing and scar formation begins and it can be divided in three progressive phases: inflammation, proliferation and remodeling. Although the tensile strength of the healing tendon improves over time, it doesn't reach the levels of uninjured, native tissue, as it can be seen in figure 2 **[7, 12, 14, 19]**.
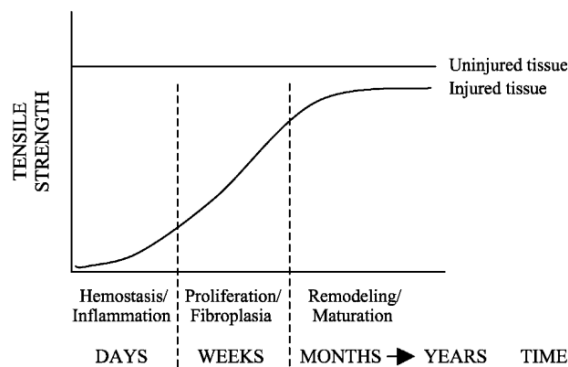
Figure 2 – Healing stages during tendon healing [19].

The first phase is the inflammatory one, it happens in the first twenty-four hours after the injury and it can be observed the formation of a hematoma; also, inflammatory cells are attracted to the injury location and fibroblasts go to the site of lesion to synthesize various ECM components **[7, 12, 14]**.

After a few days the proliferative stage begins, where fibroblasts takes several weeks to synthesize new extracellular matrix, which is mainly type III collagen and it is arranged randomly; at the end of this stage the repair tissue is highly cellular and contains a high water content **[7, 12, 14]**.

Finally, after 6 to 8 weeks, the remodeling stage begins and it may last longer than a year. This phase is characterized by the decreased cellularity and type III collagen, while type I collagen increases. Moreover, the collagen fibers start to organize, providing mechanical strength to the regenerated tissue; although the

repair tissue never achieves the functional properties of the native tendon **[7, 12, 14]**.

The healing mechanism may be intrinsic or extrinsic, or a combination of both. The extrinsic healing mechanism starts when fibroblasts and inflammatory cells go to the injury site, being responsible for the adhesion of the surrounding tissue to the damage one. The intrinsic healing mechanism results from the tenocytes proliferation level, being important for the reorganization of the collagen fibers and maintenance of fibrillar continuity **[1, 14]**.

1.6. SCAFFOLDS FOR TENDON REPAIR AND REGENERATION

Currently treatments methodologies only enable the replacement of damaged tissue with partially functionalized foreign substitutes of or pain relief. In this context, tissue engineering represents a more promising approach due to its objective to achieve full tendon regeneration. The treatment that tissue engineering offers is based on biomaterials replacement that can mimic native tissue structure and function **[1, 20, 21]**.

For this purpose, biomaterials play an important role in tissue engineering because scaffolds are made of it, being used as a temporary structure that supports the initial tissue growth. Scaffolds can enhance the tendon healing response by facilitating cell proliferation and promoting matrix production and organization into a functional tendon tissue **[3, 20, 22]**.

Tendons have special structural features that play a main role on its functions and represent a challenge on tissue engineering so, in regard to scaffold designing for tissue regeneration, there are some features that the scaffold must fulfill in order to be implanted. On the beginning of the regeneration, scaffolds must mimic tendons fibrous structure and thus its mechanical properties in order to protect the growing tissue from strong forces and to avoid an inflammatory process. Then, it should gradually be absorbed, allowing the tissue to develop more naturally and with more efficient functions, degrading at the same rate that the new tissue is created **[1, 20, 23, 24]**.

Having account the characteristics described, the scaffolding materials, ideally, should have a group of properties of the following requirements:

- Biodegradability with adjustable degradation rate;
- Maintain biocompatibility during all the degradation process and after it;
- Have similar tendon mechanical properties and maintain the mechanical strength during the tissue regeneration process;
- Be bio-functional, which means, being able to support cell proliferation and differentiation and, consequently, tissue formation;
- Have high processability, which means, being able to be easily processed in order to make complicate shapes and structures thus matching the native tissue size and shape **[1, 20, 23]**.

Therefore, one of the major goals in tissue engineering is to combine the appropriate scaffold material with cells in order to mimic the mechanical properties (stiffness, ductility, non-linearity and viscoelastic) and biochemistry of the native tendon. In the last years several materials have been used to produce scaffolds and they can be classified as biological, natural and synthetic; however few of them have the mechanical properties required to mimic the tendon tissue **[5, 15, 22]**.

1.6.1. Biological and natural scaffolds

Biological scaffolds are protein-based extracellular matrices that are normally derived from mammalian (human, equine, porcine and bovine) connective tissues. In order to remove non-collagen components, some tissues like intestine mucosa, dermis and pericardium are processed, thus minimizing the risk of rejection, while maintaining the natural collagen structure and mechanical properties **[1, 5, 25, 26]**.

Yet, the cell removal efficiency, which varies in accordance with the decellularization method, is always inferior to 100%. Moreover independently of the method, there are significant drawbacks; for example, the chemical method may leave chemicals in the final structure that can be toxic to the host cells and concerning the physical method it procedure can partially disrupt ECM structural and functional components, affecting the mechanical properties, degradation rate and bioactivity of these type of scaffolds **[1, 15]**.

Since collagen is the major ECM component in tendons, it is one of the favorite materials to be used for biological scaffolds. These scaffolds are mainly composed of naturally occurring collagen fibers (principally type I collagen) and several of them present a bioactive surface chemistry and native structure, being able to promote cellular proliferation and tissue ingrowth. Some advantages of these type of scaffolds are the 3D protein surface and the natural porosity that allows a quick interaction between the scaffold and the host tissue, inducing a faster tissue formation [1, 25, 26].

On the other hand, collagen scaffolds present some limitations such as low mechanical properties, high cost, variation from batch to batch, unpredictable degradation rate and non-defined biocompatibility, which may result in an inflammatory response and implant rejection. Some of commercially available biological scaffolds can be seen in table 1 [15, 25, 26].

For all these reasons, biological scaffolds are primarily used as surgical meshes, promoting strength and support rather than constructive tissue remodeling [27].

Concerning natural scaffolds, they are based on natural polymers that have considerable interest in tissue regeneration, when comparing with synthetic scaffolds, due to their high chemical functional groups for cellular binding and higher biocompatibility and biodegradation; some natural polymers include chitosan, silk and fibrin. However, the challenge in using natural polymer is processing them into different forms and at the same time maintain their chemical features (without chemical modification) [1, 15, 25].

1.6.2. Synthetic scaffolds

Unlike biological or natural scaffolds, synthetic scaffolds present high mechanical properties and, furthermore, they can be easily produced into different sizes and shapes, with the desired pore morphologic features and with chemical functional groups that, as consequence, induce tissue ingrowth and can meet specific mechanical and biological requirements. However, when compared with biological scaffolds, they have lower biocompatibility and many studies have revealed that they cause long time complications, such as an inflammatory response due to the body reaction to a foreign body [5, 28, 29].

Synthetic biodegradable polymers are yet preferred due to their reproducible mechanical and physical properties and the control of material impurities, presenting a predictable degradation rate [1, 23, 25].

Among synthetic polymers, the vast majority for tendon tissue engineering applications are poly(glycolic acid) (PGA), poly(lactic acid) (PLA) and their copolymer poly(lactic-co-glycolide) (PLGA), poly(ε-caprolacyone) (PCL) and poly(L-lactic acid)(PLLA). PGA fibers revealed cell and collagen alignment similar to native collagen and have the highest initial strength, but it decreases with degradation; PLGA scaffolds have been reported to improve regeneration, increasing tendon healing and PLLA presented great cell proliferation [15, 20, 23].

Between all the advantages these polymers present, they have also some disadvantages. Although their degradation products are metabolites present in the human body, they are also acidic and can produce inflammation reactions and, besides that, their structures are hydrophobic, thus don't support a high level of cell adhesion. Moreover, their biocompatibility is very poor, as they can't be absorbed or integrated into host tissue and, as a result, it may cause postoperative infection and chronic immune response [20, 23, 24].

These adverse biological reactions may be minimized when the scaffolds are small, being more appropriate for tendon repair of small defects. In table 1 can be seen some of the principal commercial synthetic devices [5, 26].

Table 1 – Commercially available scaffolds (biological and synthetic) for tendon repair [5, 26].

Scaffold Classification	Device	Material	Application	Company
Biological	Restore®	Porcine SIS	Rotator cuff, Achilles, patellar, biceps and quadriceps tendons	DePuy Orthopedics, USA
	CuffPatch®	Porcine SIS	Rotator cuff	Arthrotek, USA
	Graftjacket®	Human cadaver dermis	Foot tendons	Wright Medical, USA

	Zimmer®	Porcine dermis	Soft tissues	Zimmer, USA
	TissueMend®	Fetal bovine dermis	Rotator cuff, Achilles, patellar, biceps and quadriceps tendons	Stryker Orthopedics, USA
	Bio-Blanket®	Bovine dermis	Soft tissues	Kensey Nash Corp., USA
	OrthADAPT®	Equine pericardium	Rotator cuff and Achilles tendons	Pegasus Biologic Inc., USA
Synthetic	Gore-Tex®	Polytetrafluoroethylene (PTFE)	Soft tissues	WL Gore and Associates, USA
	Sportmesh®	Polyurethane urea (PU)	Rotator cuff	Biomet Sports Medicine, USA
	Artelon®	Polyurethane urea (PU)	Rotator Cuff and Achilles tendon	Artimplant AB, Sweden
	Leed-Kuff Patch®	Polyester	Rotator cuff	Neoligaments, UK
	Lars Ligament®	Polyethylene terephthalate (PET)	Anterior cruciate ligament and Achilles tendon	Lars, France
	Leeds-Keio®	Polyethylene terephthalate (PET)	Anterior cruciate ligament and Achilles tendon	Neoligaments, UK

CHAPTER 2 – TEXTILE STRUCTURES

2.1. INTRODUCTION

Tendon injuries are difficult to manage and although spontaneous healing can occur this often results in the formation of scar tissue, whose structure affects functionality, movement and strength of the repaired tendon. Current used therapies are mainly limited to pain control and or tissue replacement, without fully restoring tissue functionality. For the simple cases a suture backing together the tendon ends is enough. Therefore, for other cases, biological grafts may be needed to replace tissue; these can be auto or allografts, but they present some disadvantages as high donor site morbidity and functional disability, limited availability and risk of rejection **[1, 5, 10]**.

Tissue tendon engineering aims to overcome these drawbacks by regenerating a tissue with biological and mechanical properties that are similar to the native tissue. A common approach in tissue engineering involves a 3D temporary scaffold that, ideally, promotes homogeneous tissue regeneration, is biocompatible and its material can be process in order to maintain reproducibility of the 3D selected structure and high mechanical properties **[30-32].**

Like tendons, ligaments serve essential roles in joint motion, while tendons connects muscle-bone, ligaments connects bone-bone. Since, Ligament advanced reinforcement system (LARS), made of polyethylene terephthalate (PET), is one of the graft choices for ligaments rupture management, PET is a material that may have the desired properties to fulfill the tendon scaffold requirements. The introduction of these scaffolds attracted much attention because it offered benefit of quick recovery and rapid rehabilitation of the knee without severe complications often seen with other synthetic scaffolds; LARS ligament has also high mechanical strength and causes minimum complications due to the high biocompatibility **[5, 33, 34].**

In the present study, PET yarn and braided structures that will be part of the tendon scaffold structure being developed by Diana Morais under her PhD were characterized. Also, in the future, these structures will be functionalized with one of the approaches proposed in Chapter 3. These textile structures were prepared

by a textile braiding technique and fully characterized to optimize the tendon scaffold structure performing physicochemical (X-ray diffraction, Differential scanning calorimetry, swelling profile, porosity, braid angle, vertical wicking test and degradation profile) and mechanical (uniaxial tensile test) characterization.

2.2. MATERIALS AND METHODS

2.2.1. PET structures

PET yarns (1112 dTex) were purchased from Sarla Europe, LDA. Not only the properties of the PET yarn were studied, but also different braided PET structures presented in table 2 were made in order to study the influence of the number of yarns (6,8 and 16) and the take-up rate, which is the speed at which the take-up device removes the finish braid (Low, L- 1.44 cm/s and High, H – 3,94 cm/s) [35].

Table 2 – Braided structures.

Denomination	Number of yarns	Take-up rate
6YH	6	High
8YH	8	High
8YL	8	Low
16YH	16	High

2.2.2. Differential scanning calorimetry (DSC)

The thermal properites of 3 PET yarns were analysed by differential scanning calorimetric (DSC). Approximately 6 mg samples were heated from 30 °C to 290 °C (more 30 °C over melting point (260 °C) [36]) at 10 °C/min, in an aluminium pan, under a controlled argon atmosphere, using a Labsys^{TM} SETARAM instrumentation equipment.

Using the equipment software, the heats of melting (ΔHm) and cold crystallization (ΔHc) were determined by integrating the areas (J/g) under the peaks. The percent crystallinity was then determined using the following equation:

$$Cristallinity\ (\%) = \frac{\Delta Hm - \Delta Hc}{\Delta Hm^0} \times 100\ (1)$$

The term ΔHm^0 is a reference value and represents the heat of melting if the polymer was approximately 100% crystalline. In the case of PET, ΔHm^0 is equal to 140.1 (J/g) **[37, 38]**.

2.2.3. X-ray diffraction (XRD)

X-Ray diffraction (XRD) is a technique used to identify crystalline phases in materials. The PET yarn samples were analyzed on a Brucker AXS D8 Discover equipment and the data recorded using step size 0.04º and a 1 second dwell time. For the identification of each phase and determination of crystallinity, it was used software EVA.

2.2.4. Swelling profile

Swelling studies were performed in duplicate. For that, the PET yarn samples were immersed in PBS, at pH 7.4). Firstly, each sample was weighed before immersion (W_o), about 0.1 g. Afterwards, the samples were placed in a mesh and immersed in the PBS solution and incubated at 37 ºC, for 15 or 30 min. The mesh was then removed and left 5 min air drying before weighting (W_f) the PET yarn. The weight change (ΔW) of each sample represents the water absorption and was calculated using the following equation:

$$\Delta W \ (\%) = \frac{W_f - W_o}{W_o} \times 100 \ (2)$$

2.2.5. Porosity

To assess total porosity volume of the braided structures, 3 samples with 20 cm length were cut, its cross-sectional diameter ($2r$) was measured by optical microscopy in order to determine a geometrical volume ($V_g = \pi r^2 h$) and each sample was weighted (m) to determine the theoretical volume, considering a cylinder composed by 100% PET ($V_d = \frac{m}{\rho}$, considering a density of 1.3 g/cm^3 **[36]**).

Thus, the porosity percentage (P) can be calculated in accordance with the equation 3:

$$P \ (\%) = \frac{V_g - V_d}{V_g} \times 100 \ (3)$$

2.2.6. Braid angle

To measure the braid angle, each braided structure was observed at the optical microscope and the images were obtained through the microscope software. After that, braid angle was measure through the software *J image*.

2.2.7. Vertical wicking test

The vertical wicking test was performed three times using three samples per test. PET specimens of 20 cm length were suspended vertically with its bottom end dipped in a reservoir of distilled water with a color agent. In order to ensure that the bottom ends of the specimens could be immersed vertically at a depth of 3 cm into the colored water, the bottom end of each specimen was clamped with a clip (the apparatus can be seen in figure 3). The wicking heights, measured every minute over 10 min, were recorded for a direct evaluation of the PET structures wicking ability.

Figure 3 – Vertical wicking test apparatus.

2.2.8. Tensile test

The uniaxial tensile tests of the braided structures were performed (in triplicate) on LR 30K from Lloyd instruments. The distance between the jaws was 200 mm, and the speed applied was 10 mm/s, which mimics the velocity of a real walking situation. During the tests, mechanical properties such as maximum load and maximum strain of all structures were obtained **[17]**.

2.2.9. Yarn degradation

PET yarn degradation studies were performed in 2 mL PBS (pH 7.4), in triplicate, where initial weight was recorded. All samples were then incubated at 37 °C and 60 rpm agitation. After 15 days and 1 month the PET yarn samples were removed, dried and weighted. It was also performed a tensile test with the parameter indicated before.

2.3. RESULTS AND DISCUSSION

2.3.1. DSC

Crystallinity is a well-known material variable that affects not only the physical–mechanical properties but also biodegradability. For this reason, is important to trace the "as received" PET yarn crystallinity, to study in the future its influence on the scaffold properties [39].

In Figure 4 it can be seen a DSC curve for a PET yarn sample, showing the heat flow variation over temperature.
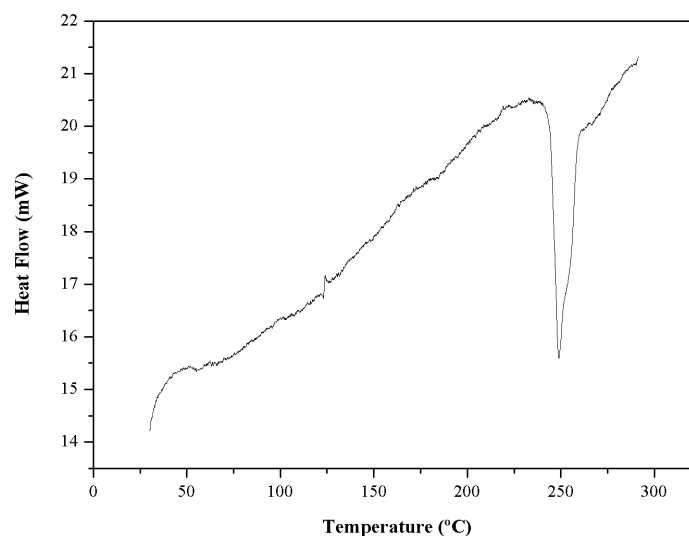
Figure 4 – DSC of the PET yarn.

As it can be seen, the endothermal peak represents the melting temperature of the material, which is around 250 °C and, the exothermal peak is related with the cold crystallization temperature around 123 °C. These values are in accordance with the literature [40, 41]. The glass transition temperature is reported to vary from 70 to 114 °C [40]., but no defined peak could be observed in this region. This may be explained due to the "noise" of the acquisition data; due to the heating rate being too low, in which this kinetic transition causes a too small effect, it could not be detected [42].

Using equation 1 it was possible to estimate the PET yarn crystallinity degree, which was approximately 53 ± 2,4 %, that is in agreement with the literature being a semi-crystalline polymer **[41]**.

2.3.2. XRD

From figure 5 it is possible to observe the PET yarn XRD spectra.
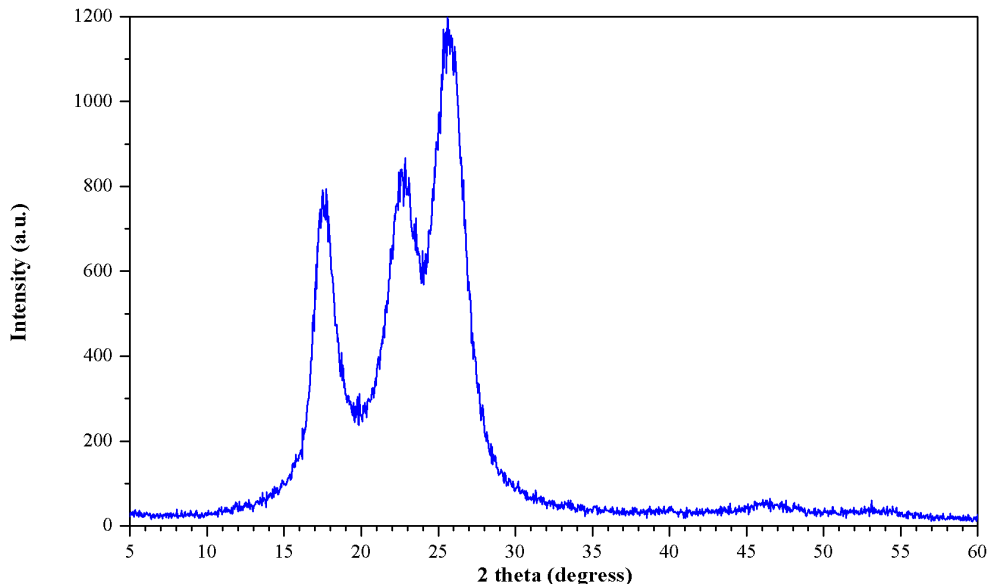
Figure 5 – XRD spectrum for PET yarn.

The XRD pattern of the PET yarn displays reflections characteristics of crystallinity relative to planes (010), (110) and (1000), for scattering angles 2θ = 17.6 °, 22.8 ° and 25.6 °, respectively. The peaks observed are characteristic of PET and have also been observed by other authors **[43, 44].**

Moreover, through this technique it was also estimated the PET yarn crystallinity being approximately 55 ± 3,2 %, which is in accordance with the DSC crystallinity result.

2.3.3. Swelling profile

The PET yarn weight change over time is illustrated in figure 6, representing its water absorption. This study was done using a PSB solution at 37 °C order to mimic the physiological conditions and see the PET yarn swelling over time **[45]**.
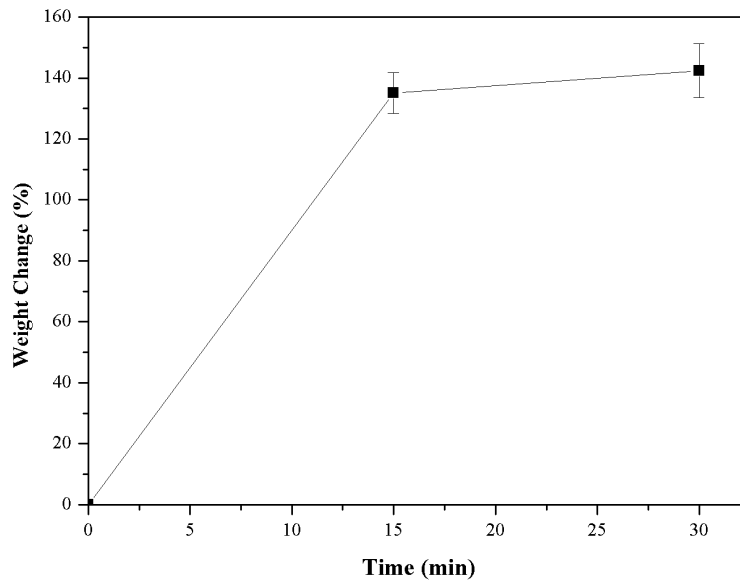
Figure 6 – Weight change over time of the PET yarn at 37 °C, immersed in a PBS (pH 7.4) solution.

It is believed that swelling occurs as a result of water entering in order to reduce the osmotic pressure. Water molecules diffuse into the amorphous regions of the yarn and break inter-molecular hydrogen bonds, allowing an increase in the inter-molecular distance of the polymer chains, which causes swelling. As a result, swelling increases the amorphous regions of the yarn **[46, 47]**.

Since the PET yarn weight changed over time (Figure 6), it means that yarn swelling occurred due to the water diffusion into the yarn, leading to an increase of weight and thus water absorption. Observing figure 6, at an initial stage there was significant water absorption, causing a weight increase of 135% after 15 min of immersion and then the swelling rate decreased up to 30 min, achieving a weight change of 142%. The increase of swelling over time means that the void regions of the yarn are still being filled until it reaches the saturation point, where the equilibrium state is reached, where the osmotic pressure is balanced by the forces of the crosslinking bonds **[46, 48]**.

2.3.4. Porosity

Scaffold porosity can modulate the functionality and cellular response to the implant. Pore interconnectivity extending through an implant increases the overall surface area for cell attachment, which can enhance the regenerative properties of the implant by allowing tissue ingrowth into the interior of the matrix. Figure 7 shows the porosity results of the braided structures being study **[49, 50]**.
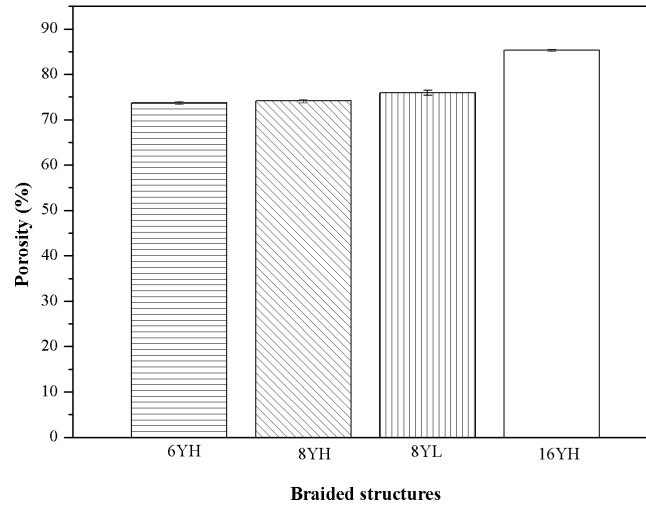
Figure 7 - Porosity of the different braided structures.

Regarding the number of yarns, it can be seen that a high number led to a high porosity, especially from 8YH to 16YH increasing from around 74% to 85%. This difference between these two structures may be even more accentuated because increasing the number of yarns increases the void spaces since there is more void spaces interyarn. However, comparing 6YH with 8YHno significant difference is detectable as well as no effect was observed by changing the take-up rate (8YH vs 8YL).

2.3.5. Braid angle

The braid angle is half the angle of the interlacing between the two sets of yarns of a braid (in figure 8 it can be seen the measurement performed for each braid structure) and defines the resulting braid geometry. The ratio of the speed of the yarn to the take-up device that removes the finished braid determines the braid angle so, controlling the take-up rate it is possible to define the braid angle (yarn orientation) **[35, 51]**.
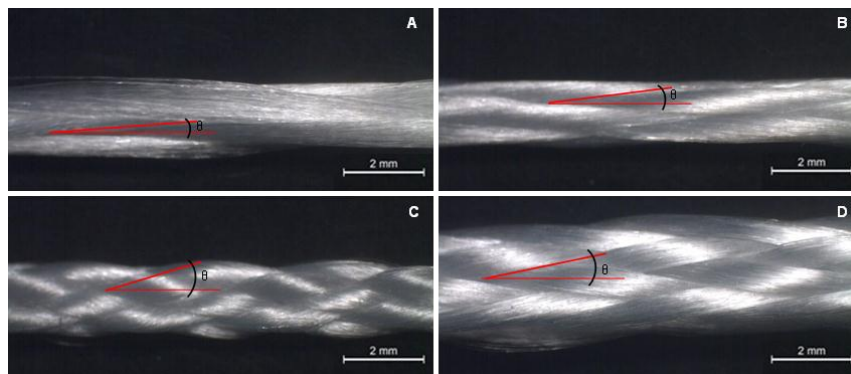
Figure 8 - Braid angle measure: a) 6YH; b) 8YH; c) 8YL and d) 16YH.

In order to optimize the braided structure properties to be similar to a tendon one, it is important to study the braid angle variation because it will have effect on the braid porosity and on its mechanical properties **[52, 53]**

In figure 9 it is possible to analyse the influence of the number of yarns and take-up rate on the braid angle.
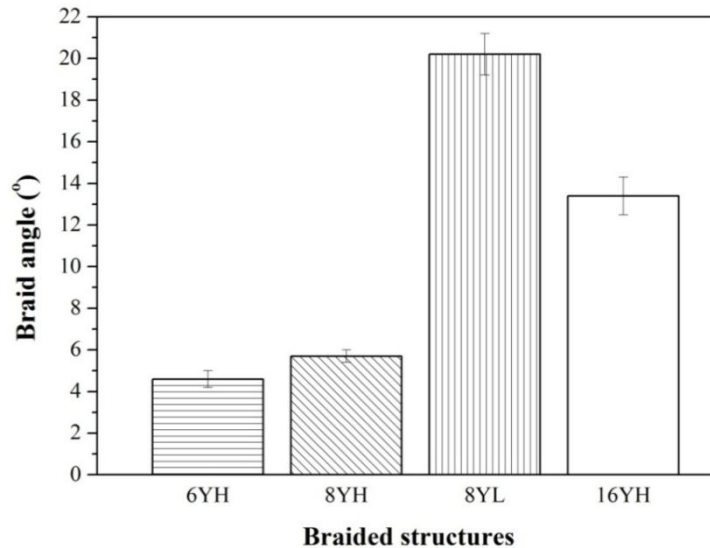
Figure 9 - Braid angle of the different braided structures.

Observing figure 9, samples 8YH and 8YL demonstrated the take-up rate influence in the braid angle, which significantly increases for the a lowest take-up rate, from approximately 6 ° to 20 °. Moreover, for the same take-up rate (6YH, 8YH and 16YH), a significant increase of the number of yarns will lead to an increase of the braid angle. Between the structure with 6 and 8 yarns, there is no significant difference being achieved a value of 5° and 6°, respectively; on the other hand, the structure with 16 yarns presented a braid angle of 14°.

The results obtained are confirmed by the literature that describes the effect of the take-up rate and number of yarns on the braid angle, referring that increasing the number of yarns will increase the braid angle and that lowering the take-up rate will also increase the braid angle **[53]**.

2.3.6. *Vertical wicking test*

One of the scaffolds limitations is the ability to promote cell infiltration and oxygen and nutrients diffusion which is important to ensure cell attachment, proliferation and differentiation. The scaffold design is a way to overcome these

limitations and it has been proved that a high wicking ability increases fluid intake and enhance cells infiltration and distribution **[54-56].**

Figure 10 shows the vertical wicking curve, namely the capillary rise vs time, for PET yarn and braided structures varying the number of yarns maintaining a lower take-up rate (figure 10-a), and varying the take-up rate maintaining a structure with 8 yarns (figure 10-b).
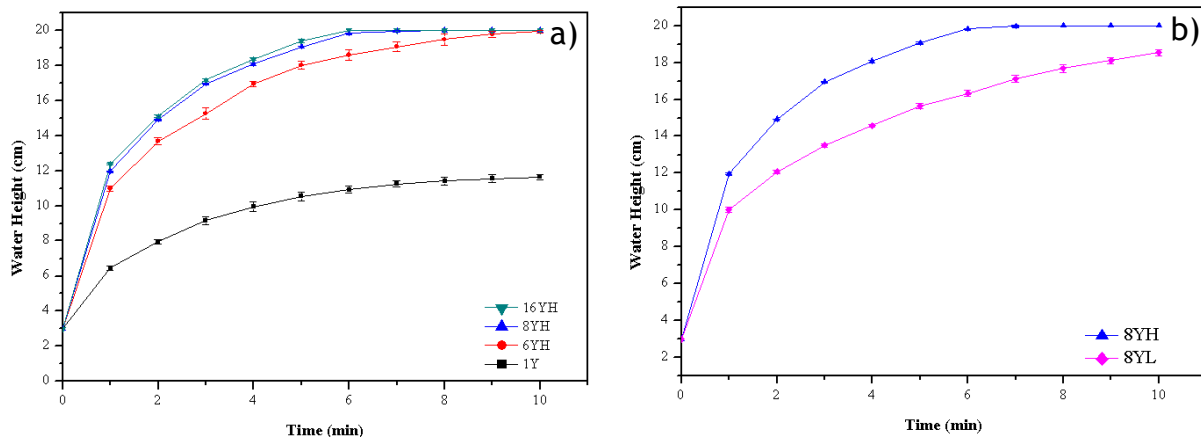
Figure 10 – Vertical wicking curve: a) varying PET structures number of yarns; b) varying PET structure take-up rate.

Capillary rise within a textile is influenced by a number of factors, especially by the fabric structure (porosity, yarn content and braid angle, for example), being related with the water height in the yarn. It is evident from the capillary rise shown in figure 10-a that using a braided structure instead of a single yarn results in an increase of the capillary ability at 10 min from 11 cm for 1 yarn structure to 20 cm for the other structures **[57].**

Moreover, from figure 10-b it is possible to conclude that a high take-up rate velocity (8YH) resulted in a high capillary rise because at 6 min while the highest take-up rate structure already reached 20 cm height, the structure produced with a lowest take-up rate (8YL) only reached 15 cm.

Capillary wicking is a liquid transfer mechanism which is determined mainly by effective capillary pore distribution and pathways, being the spontaneous flow of the liquid due to the capillary spaces between yarns **[58, 59]**.

The structure geometry influences the pore size and the quality of the capillary channels in the inter yarn spaces. Moreover, the yarns density and structure have an influence in the inter- and intra- yarns pores dimension and distribution along the fabrics **[58].**

21

A structure with more capillary spaces will have a high capillary rise. This is in accordance with the porosity, since structures with more yarns have a high porosity and thus have a high and fast capillary rise. Regarding the structures produced with 8 yarns, the one produced with the lowest take-up rate (8YL) presented a much low capillary rise. However since the 8YH and 8YL porosity is similar that means the braid angle has a high importance on the capillarity. Since the number of yarns is the same and the braid angle is higher for the 8YL sample, the pores may not be at the capillary level but macro pores causing low capillary pressure. Literature reported this phenomenon [55], where different macro-pore sized scaffolds where studied and found that the smaller the pore size the higher the fluid rise.

2.3.7. Tensile test

In order to mimic the native tendon mechanical properties, the scaffold must have similar mechanical properties. Figure 11 presents the braided structures tensile test curves and figure 12 presents the mechanical properties for each structure studied [28].
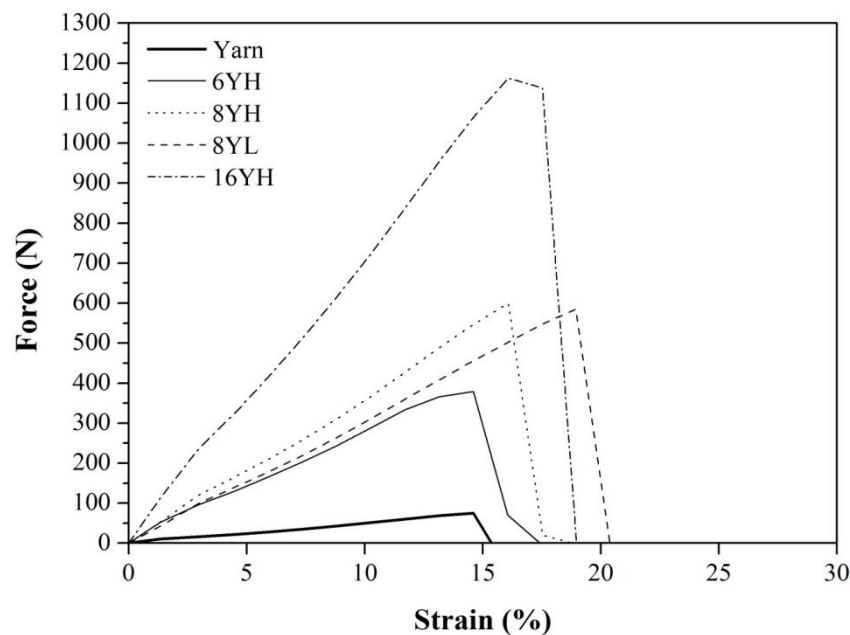
Figure 11 – Tensile test results for the different PET structures.

22
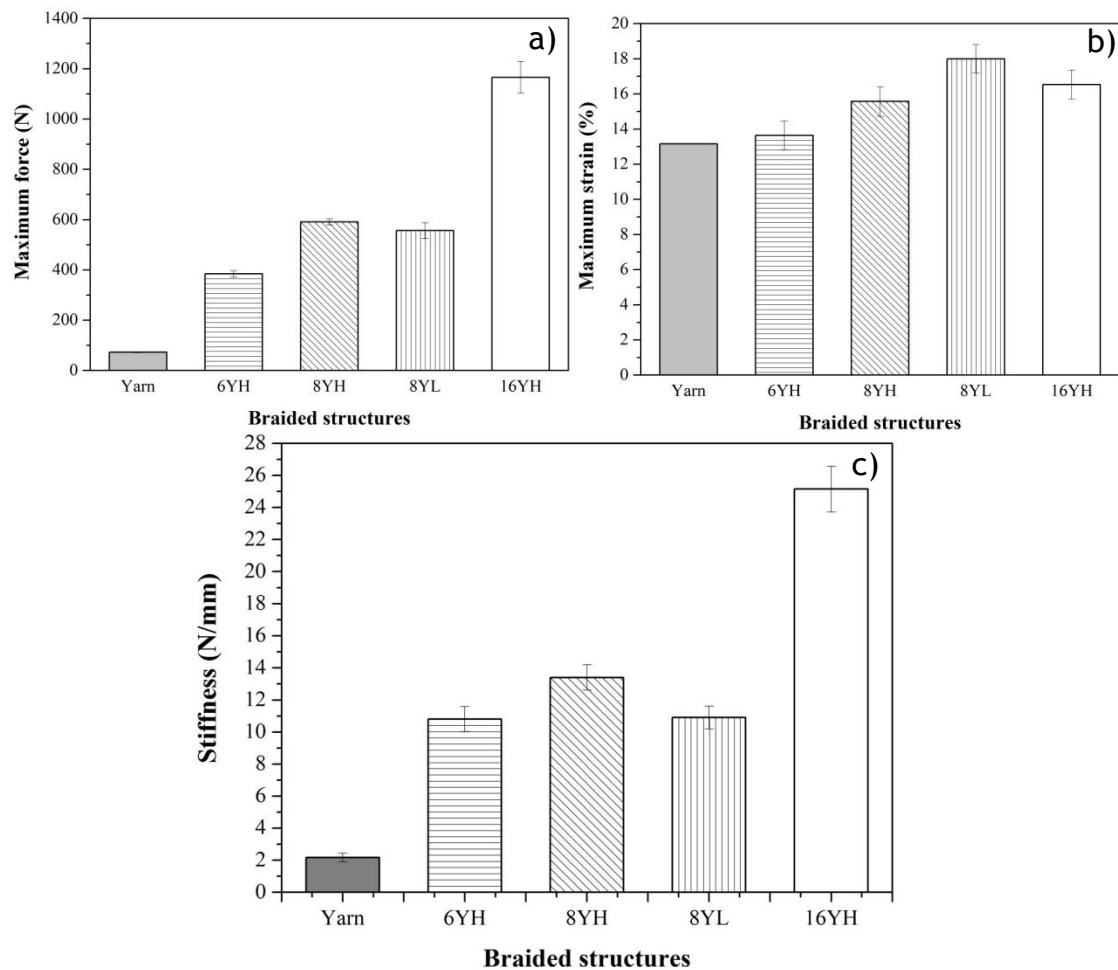
Figure 12 – Structures mechanical properties: a) maximum force, b) maximum strain and c) stifness.

Observing figures 11 and 12-a and b, concerning the number of yarns, a braided structure with high number yarns presents a high maximum force before rupture, being from around 50N for 1 yarn to 1200 N for 16YH structure. The same behavior is observed for the maximum strain achieved before rupture, being from around 13% to 17%, for 1 yarn and 16YH structures, respectively. The maximum load increases with the number of yarns because the load applied is divided through all the yarns.

Regarding the take-up rate variation, no significant difference was observed for the maximum force, being around 600 N for both structures (8YH and 8YL). Concerning the maximum strain, it was considerably higher for the lower take-up rate, varying from around 16% to 19% for 8YH and 8YL, respectively. In this case, the maximum strain is mainly influence by the braid angle, where a high braid angle (8YL) led to a maximum strain because, as have been reported on the literature, structures with a high braid angle have initially a low parallel alignment

of the yarns, so it will take more time to align in axial direction the yarns and therefore present high maximum strain **[35, 60]**.

Besides the 16YH sample, for all the other the maximum load and strain corresponds to the yield point because after this point the force applied decrease meaning that fracture occurred. In the case of 16YH sample, the yield point is around 1130 N.

The maximum force applied to Achilles tendon during a slow walk is of 2600 N and up to 9000 N during running. Although the rupture force of braided structures being studied is bellow these values, the final structure being developed by Diana Morais will have several of these structures associated in order to achive the native tendon mechanical properties **[4]**.

Tendons are stiff (force required to stretch it on unit distance) and present high tensile strength. Therefore, the structures stiffness was also studied. **[4, 61]**.

Figure 12-c presents the stiffness value of the different PET structures, that was calculate on the *linear region* of the curve, between 2% and 6% strain. Like for the maximum force achieved, the stiffness increased with the number of yarns from 2 N/mm to 25 N/mm for the 1 yarn and 16YH structures, respectively. Moreover, the stiffness decreases with the take-up rate, varying from 14 N/mm to 11 N/mm for 8YH and 8YL structures, respectively.

Increasing the number of yarns, for similar strain level, more force was needed to be applied thus leading to a high stiffness. Between the structures with different take-up rate, in the one with the lowest braid angle (8YH) the yarns tend to align to the axial direction, thus low strain will occur and the stiffness in axial direction increase **[62]**.

Having in account the tendon properties referred, the structure that present more promising results to be used in the tendon scaffold is the 16YH structure.

2.3.8. Yarn degradation

Developing scaffolds with the optimal characteristics such as an adequate degradation rate is important to assure for example that the strength of the scaffolds is maintained until the regenerated tissue takes over the synthetic scaffold **[63]**.

After each PET yarn immersion time, no weight loss was observed, indicating that no significant degradation occurred.

Moreover, figure 13 shows the tensile test curve of the PET yarn for each degradation test time, in order to analyze mechanical properties alterations.
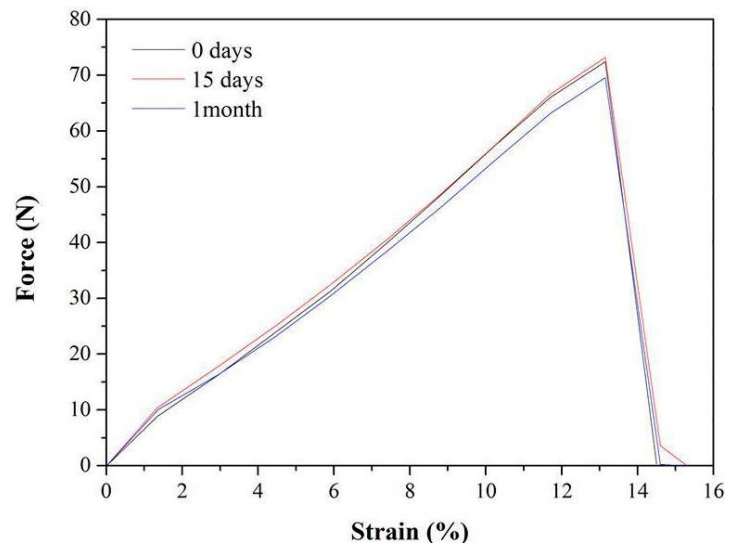
Figure 13 - Tensile test results of PET yarn, for each immersion time.

Observing figure 13, the maximum force and strain achieved after each immersion time (15 days and 1 month) is similar to the PET yarn that didn't suffer immersion, approximately 75 N and 13% strain. These results indicate that the PET yarn may be suitable to be used in a tendon regeneration scaffold since it maintained its mechanical properties after 1 month of immersion.

CHAPTER 3 - SURFACE FUNCTIONALIZATION OF POLY(ETHYLENE TEREPHTHALATE)

3.1. INTRODUCTION

Because the majority of the biological reactions take place at the interface between biological systems, surfaces play an important role in biology and medicine. In tendon tissue engineering, the chemical and physical properties of the scaffold surface must promote good cell attachment, proliferation and differentiation, to finally organize the matrix into a functional tendon **[20, 64]**.

Polymeric materials provide support surfaces for the immobilization of biologically active molecules and living cells, having many applications in the field of tissue engineering. However, the use of various polymeric materials is drastically limited due to their inert and hydrophobic surface, which affects cell adhesion and proliferation **[5, 15]**.

PET is a linear aromatic polymer, with excellent bulk properties, such as high specific strength, good resistance to corrosion and it is relatively inexpensive to produce. Though, PET is inert, lacking active functional groups and is non-degradable. Moreover due to its low surface energy, it has poor wettability and cellular adhesion **[20, 64]**.

It has been some interest in adding functional groups to non-degradable synthetic graft surfaces in the expectation of enabling new tissue growth and integration, and avoids immunological reactions to the foreign body and high failure rates **[64]**.

Several physical and chemical approaches have been developed to modify scaffolds surface. Among them, plasma treatment is frequently used to improve wettability, more specifically, oxygen plasma treatment causes the formation of oxygen groups on the polymer surface (polar functional groups), such as C-O, C=O and O=C-O, increasing their hydrophilicity. Moreover, the formation of amine groups (NH_2) was shown to be a good mean to improve cell adhesive properties **[64-66]**.

An alternative to plasma treatment for the introduction of amino groups on the polymer surface is a chemical etching on the form of aminolysis using diamines. Aminolysis has been demonstrated to be effective for modifying polymeric scaffolds or membranes for tissue engineering applications, where the free amino groups were used as a chemical linker to immobilize macromolecules, such as gelatin, chitosan and collagen **[67]**.

On the particular case of ethylenediamine (EDA), the amino groups (-NH$_2$) can be chemisorbed on PET substrats via –C(O)NH- bonds by EDA modification in water solution; it couples to the polymer surface by one amine side only, leaving other available to react **[68]**.

Another approach is using a coating with adhesion molecules, such as poly-D-lysine, that has been used to enhance adhesion and growth of cells on the scaffold. Due to its cationic nature, poly-D-lysine is an attractive coating for the adherence of the cells because it enhances electrostatic interaction between negative charges of the cell membrane and positively-charged ions. Moreover, when comparing with other ECM components, it has a smaller cost **[69]**.

In the present study, the PET surface was functionalize, first by plasma activation (oxygen and argon plus oxygen) and afterwards by incorporating amine groups by two approaches: 1) with a wet treatment ethylenediamine aminolysis and 2) with the adhesion molecule, D-lysine. The surface modifications were characterized by assessment of the water contact angle, total reflection fourier transformation infrared (FTIR-ATR) spectroscopy, Atomic Force Microscopy (AFM), Scanning electron microscopy (SEM) and colorimetric staining with Acid Orange II.

3.2. MATERIALS

PET membrane biaxilly oriented whit 0.1 mm thickness (ref. ES301400, Goodfellow), Ethylene diamine (EDA) (99%) (ref. E26266, Sigma), D-lysine hydrochloride (99%) (10435295, Acros Organics), distilled and deionized water, Phosphate buffered saline (PBS), ethanol (96%), isopropanol (99%), NaOH (0.1 and 1 M), HCl (1 M), orange 7 (ref. 633-96-5, Acros Organics), L929 cell lines (ATCC CCL-1™), α-MEM (Gibco, Invitrogen No. 11900-073) , fetal bovine serum (Gibco Invitrogen No. 10106-169), penicillin and streptomycin solution (Gibco Invitrogen

No. 15140-122), fungizone (Gibco Invitrogen No. 15290-026), glutaraldehyde (0.14 M), sodium cacodylate buffer (pH 7.4)

3.3. METHODS

3.3.1. Surface functionalization

3.3.1.1. PET sample preparation

All processes were performed on circular PET membranes with 0.1 mm thickness and 25 mm diameter in dimension, except for AFM and SEM analysis, that were performed in PET membranes with 13 mm diameter. Before all plasma activation treatments, the PET substrates were cleaned with ethanol.

3.3.1.2. Plasma treatment

A Zepto laboratory-sized plasma system from Diener Electronics (ø = 105 mm, L = 300 mm, V = 2.6 L) was used for the plasma activation of the samples. Several plasma treatments were performed, taking into account the effect of two main parameters: used gas and plasma treatment time. Based on these parameters, three combinations of these parameters were used:

1. Oxygen gas treatment (2 to 10 min, 100 W);
2. Mixture of Argon and Oxygen (2 to 10 min, 100 W);
3. Argon pre-treatment (2 min, 100W) and then only oxygen treatment (2 to 10 min, 100W).

3.3.1.3. Grafting approaches

a) EDA grafting

Immediately after the plasma treatment, PET samples were immersed in different EDA solutions for 24 h as shown in table 3.

Table 3 - EDA grafting conditions.

Denomination	Solvent	Temperature (ºC)	EDA concentration (v/v)
W2025	water	20	25%
W2050			50%
W5050		50	50%
E2025	Ethanol	20	25%
E2050			50%

After the grafting treatment, all samples were removed from the reactive solutions, rinsed firstly in distilled water, then in isopropanol and again in distilled water. Finally, the grafted samples were dried under vacuum condition at room temperature before analysis.

b) D-Lysine grafting

Immediately after plasma treatment, PET samples were immersed in D-lysine solution 0.04 (g/ml) at 37 °C, for 2 h, using PBS as a solvent for the pH 7 solution and using deionized water for the pH 9.5 solution (using 0.1 M NaOH to adjust the pH). After the treatment, all samples were removed from reactive solutions and rinsed three times with PBS. Finally, the grafted samples were air dried before analysis.

3.3.2. Physico-chemical characterization

3.3.2.1. Differential scanning calorimetry (DSC)

The DSC test procedure was the same described on chapter 2, but applied to 10 mg PET membrane samples.

3.3.2.2. Contact angle

The wettability of PET after plasma activation and after surface grafting was assessed by the sessile drop method, measuring the water contact angle on the samples using a 3 μl drop of deionized water, at room temperature using a OCA 20 unit from Dataphysics. A minimum of six contact angle measurements were performed for each condition.

3.3.2.3. Fourier transform infrared – attenuated total reflectance (FTIR-ATR) spectroscopy analysis

The chemical bonding characteristics were analysed by Fourier Transform Infrared Spectroscopy (FTIR) in Attenuated Total Reflectance (ATR) mode, using a Jasco FT/IR 4100 system. All ATR-FTIR measurements (64 scans, 8 cm^{-1} nominal resolution) were performed immediately after the plasma activation and grafting of the samples.

3.3.2.4. Atomic Force Microscopy (AFM)

The surface topography, average roughness (R_a) and surface height standard deviation (R_q) of the PET substrates were assessed before and after the plasma activation and after surface grafting using a Multimode Atomic Force Microscope (AFM) from Digital Instruments using the tapping mode (scan size 5 x 5 μm^2 and scan rate 1 Hz). A Nanoscope III controller and Tesp AFM tips from Bruker were also used.

3.3.2.5. Optical Profilometer

The surface profilometry was performed using a *Bruker*, model *NPFLEX* equipment.

3.3.2.6. Scanning electron microscopy (SEM)

In order to evaluate the samples surface morphology, SEM analysis was performed in a Quanta 400FEG SEM microscope (FEI, USA), after a gold-paladium coating of the samples using a SPI sputter coater.

3.3.2.7. Evaluation of amino group density (Acid Orange II)

To quantify the amount of exposed primary amine groups after PET surface grafting, the Orange II method was used. The amino-covered samples were immersed on 3 mL of acidic dye solution (14 mg/mL) (adjusted to pH 3 with 1 M HCl) and shaken for 1 h at 40 °C. The samples were then thoroughly rinsed three times with water acidic solution (pH 3) to remove unbound dye. Once air-dried, the colored samples were immersed in 2 mL of water adjusted to pH 12 with a 1 M NaOH solution and shaken for 15 min at room temperature. The absorbance of the solution was then measured at 485 nm.

3.3.3. Cell viability evaluation

3.3.3.1. Resazurin assay

L929 cell line was cultured in α-MEM (supplemented with 10% (v/v) fetal bovine serum, 1% penicillin and streptomycin solution and 2.5 µg/mL of fungizone. Cells were seeded at $2x10^4$ cells per well (24-well culture plates) on the samples surface (untreated PET substrate and EDA (W5050) and D-Lysine (pH 9.5) grafted PET substrate) for 1, 3 and 7 days at 37 °C, in a 5 % CO_2 humidified atmosphere. After each time point, 50 µl of resazurin at 37 °C were added to each well and the plates

were incubated for 3 hours at 37 °C in a 5 % CO_2 humidified atmosphere. Then, the fluorescence was measured at 595 nm using a microplate reader. This experiment was performed in triplicate.

3.3.3.2. SEM analysis

The morphology of L929 fibroblasts seeded on the surface of untreated, EDA treated (condition W5050) and D-Lysine treated (pH 9.5) PET, after each time point was analysed by SEM. Briefly, samples with cells were firstly washed twice with PBS and fixed with 1.5 % (m/V) glutaraldehyde in 0.14 M sodium cacodylate buffer (pH 7.4) over 15 min. Afterwards, samples were dehydrated using graded ethanol solutions from 50 % (V/V) to 100 % (V/V). The samples lasted 10 min in 70 and 80% ethanol solutions, 20 min in 90% ethanol solution and overnight in 100 % ethanol solution. Finally, samples were placed onto aluminum stubs and coated with gold/palladium using a sputter coater (SPI, USA) for SEM analysis in a Quanta 400FEG SEM microscope (FEI, USA).

3.4. RESULTS AND DISCUSSION

3.4.1. DSC

In Figure 14 it can be seen a DSC curve for a PET membrane, showing the heat flow variation over temperature.
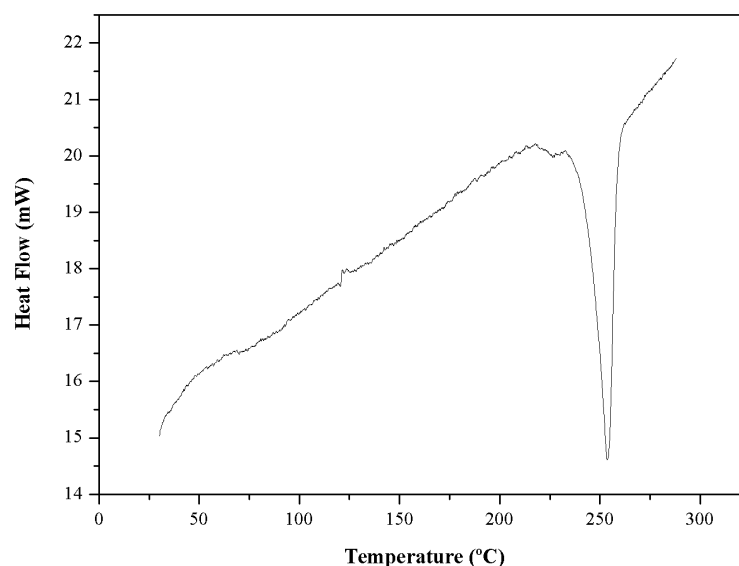

Figure 14 – DSC of PET membrane.

As it can be seen, the endothermic peak represents the melting temperature of the material, which is around 254 °C and the exothermic peak is related with the

cold crystallization temperature around 121 °C. These values are similar to the ones described for the PET yarn and are in accordance with the literature. Once again, for the same reasons described before, the glass transition temperature is not visible.

Using equation 1 it was possible to calculate the PET membrane crystallinity degree which was approximately 41 ± 1,8 %, being more amorphous than the PET yarn.

3.4.2. Plasma treatment

For PET surface activation, oxygen and argon plus oxygen plasma treatment gases were chosen to decrease its hydrophobicity and create new functional groups. Oxygen was chosen in order to activate the surface, anchoring groups such as carboxylic and hydroxyl and all conditions tested have used this gas because it creates more groups that allow a better amines grafting. Argon was used as a gas to clean the material surface and alter the surface morphology **[70, 71].**

3.4.2.1. Contact Angle

In order to enhance the further surface functionalization it is important to have an initial surface with low contact angle to allow the solution to wet the surface and obtain a more homogenous coating. To optimize the surface activation process parameters and to obtain a suitable gas or gaseous mixture, treatments were carried out at varying exposure times. In figure 15 is possible to observe the water contact angle variation as function of each plasma treatment conditions.

All treatments led to the improvement of the hydrophilicity of the samples, causing a water contact angle decreased.This increase in the wettability is generally attributed to the introduction of chemical polar groups, such as carboxyl (-COOH) and hydroxyl (-OH), with hydrophilic behavior on the polymer surface **[72].**
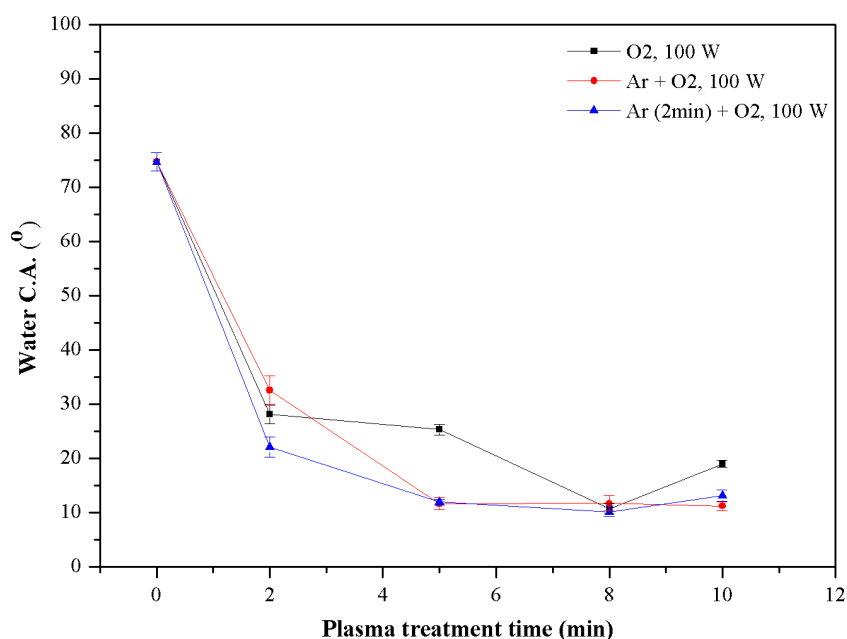
Figure 15 – Water contact angle (θ) for different plasma treatment conditions.

The results presented in figure 15 show that for all conditions it is evident a decrease of θ over plasma treatment time and the lowest θ values for all the treatments were achieved at 8 min. At 8 min treatment it was observed a decrease from 74.7 ° to 10.7 ° for the treatment with only oxygen gas; 11.7 ° for the mixture of argon and oxygen and 10.13 ° for the treatment with 2 minutes argon plus 8 minutes oxygen. Similar trends were reported in the literature for different polymers after treatments under atmospheric pressure **[57, 72].**

Between the three plasma treatment conditions, although all present a θ decrease over plasma treatment time for the conditions with argon this phenomenon is more evident for the lowest treatment times, This may happen because the material surface is less contaminated and its roughness has been changed, enhancing oxygen plasma activation. At 8 min treatment, the argon gas effect over oxygen gas is minimum, reaching a similar θ.

Based on these results, the conditions that were chosen for further surface characterization were the 8 min oxygen plasma treatment after 2 min argon and 8 min oxygen plasma treatment. The treatment with gases mixture was excluded because since the gases are pumped at the same time there would be a low oxygen concentration at the plasma chamber and this gas was important for chemical surface activation.

3.4.2.2. FTIR-ATR

Figure 16, shows the FTIR-ATR spectra of PET, untreated and after the selected plasma treatment conditions (with oxygen gas, figure 16-a, and with argon plus oxygen gas, figure 16-b). Using this technique no detectable changes were observed among spectra before and after the plasma treatments performed.
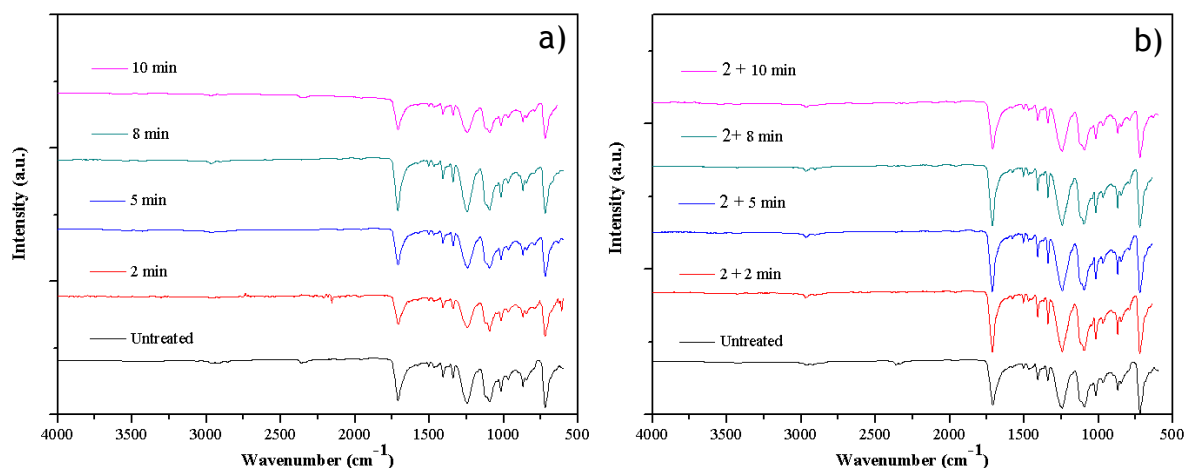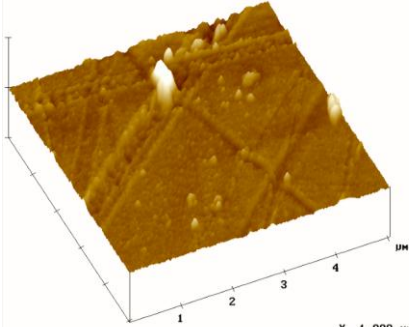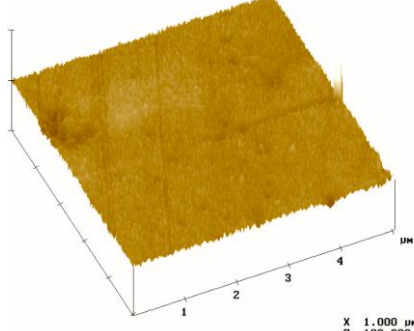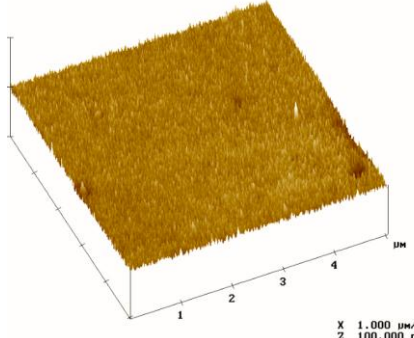
Figure 16 – FTIR-ATR spectra of untreated and plasma treated samples. a) samples activated with oxygen gas and b) samples activated with argon plus oxygen gases.

3.4.2.3. AFM

In order to see the effect of the plasma treatment on the surface roughness, the treated samples were analysed by AFM. Table 4 shows the average roughness (R_a), standard deviation of surface heights (R_q) and a representative 3D height images for the different conditions.

Table 4 – AFM results for untreated and plasma treated samples.

Treatment	Sample	R_a (nm)	R_q (nm)
Untreated		3.4 ± 0.5	5.8 ± 1.5

8 min O$_2$		2.9 ± 0.6	4.4 ± 0.9
2 min Ar + 8 min O$_2$		3.3 ±0.6	4.6 ± 1.0

As it can be seen in table 4, the surface average roughness didn't changed significantly between the untreated sample and both plasma treatments. On the other hand, the treated surfaces seem to be more homogenous, being the peaks more uniformly distributed and with similar height.

On the plasma treated samples, although the surface topography changes may have contributed to the water contact angle decrease (see figure 15), the maintenance of the average roughness indicates that the significant hydrophilicity increase is mainly due to the chemical activation on the surface, which means that the creation of new functional groups on the PET surface may have been successfully achieved.

3.4.3. EDA grafting

In order to understand the reaction between EDA and PET surface, figure 17 represents a scheme of the reaction, showing how the grafting occurs.
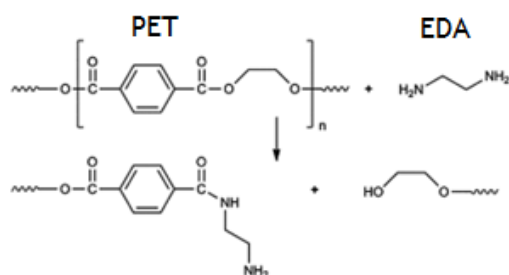
Figure 17 – Reaction scheme between PET and EDA [68].

Based on FTIR-ATR and acid orange results, only the EDA grafting conditions that revealed to be more interesting were chosen to be analysed (W5050 and E2050) because the other conditions didn't present amino group characteristic peaks (see figure 32 from attachments) and the acid orange method demonstrated low amino group density (see figure 20).

3.4.3.1. FTIR-ATR

Figure 18, shows the FTIR-ATR spectra of PET, untreated and after the EDA grafting conditions W5050 and E2050, using oxygen and argon plus oxygen plasma (figure 18-a and figure 18-b, respectively).
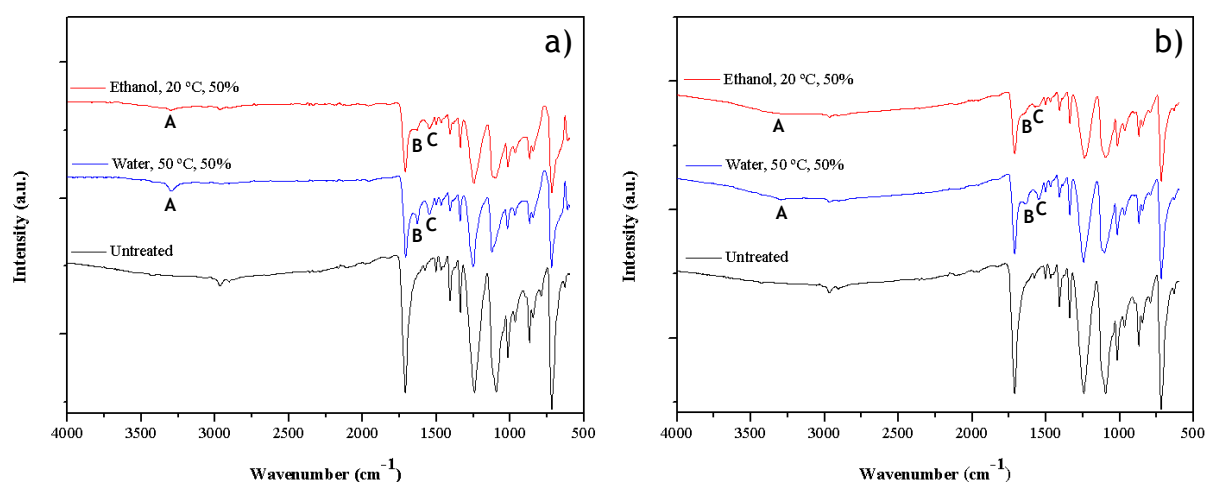
Figure 18 – FTIR-ATR spectra of untreated PET and EDA grafted samples (W5050 and E2050): a) samples activated with 8 min oxygen plasma and b) samples activated with 2 min argon and 8 min oxygen plasma.

In the FTIR-ATR spectra of the PET surface after EDA treatments new bands characteristic for amine, amide and hydroxyl groups were expected according to reaction shown in figure 17; in figure 18-a can be seen that the treated samples have a new peak at 3300 cm^{-1} (A) that corresponds to the stretching vibration of amine I and II. The region 1750–1500 cm^{-1} is also rich in new peaks, being the 1630 cm^{-1} (B) and 1546 cm^{-1} (C) peaks the amide I and amide II stretching bond

36

respectively, which confirms the presence of -CONH bonds on the PET surface, which were obtained after plasma activation. The appearance of these peaks is related with the presence of EDA, indicating that EDA has been linked to the PET surface [73].

Between oxygen plasma treatment (figure 18-a) and argon plus oxygen plasma treatment (figure 18-b), although the argon plus oxygen treatment presents the same new peaks described previously between 1750-1550 cm^{-1}, they are less intense and also the peak at 3300 cm^{-1} barely appears, indicating less quantity of amine groups for this type of plasma treatment. Moreover, for each plasma treatment conditions, when comparing W5050 and E2050 samples, both present similar peak signals, however the signal is more intense for the W5050 sample, which indicates the presence of more amino groups.

3.4.3.2. Amino groups density

From figure 19 it is possible to compare the primary amine group density for each plasma treatment and EDA grafting condition.
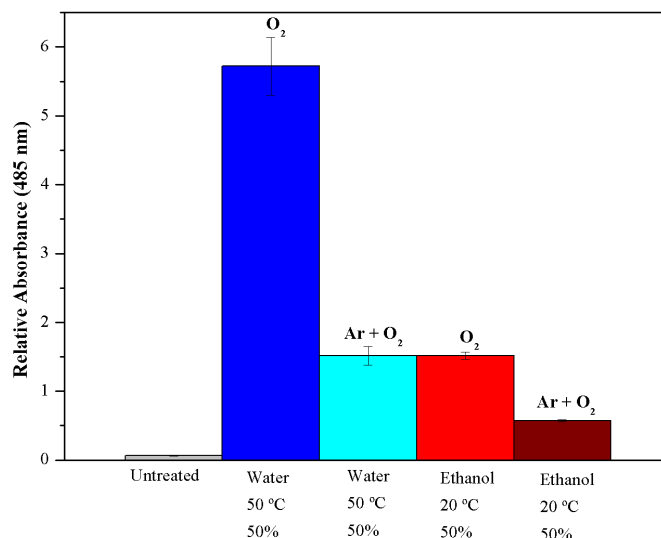
Figure 19 – Amino group density on untreated PET sample and EDA grafted samples (W5050 and E2050), for each plasma treatment, based on acid orange absorbance.

Comparing the untreated sample with the treated ones, all the treatments result in an increase of the acid orange absorbance meaning an increase of the amine groups density. This behavior was expected because the PET chemical structure doesn't present any amine group and with the EDA treatment the amine groups were introduced in the PET surface (see figure 17).

When comparing the two plasma treatment conditions, the oxygen plasma treatment presents a higher amine density for both EDA treatments than the argon and oxygen treatment. These results are in accordance with the FTIR-ATR results, where amine group peaks appeared and were more intense for oxygen plasma treatment than for argon plus oxygen treatment (see figure 18). This may occur because when using argon before oxygen the chamber is not empty and since argon has higher molecular weight than oxygen it doesn't allow the oxygen entrance. In consequence, less oxygen will be pumped into the chamber and react with the surface, creating less functionalizing groups.

Between the W5050 and E2050 samples the amine group density in W5050 is higher than in E2050; varying, respectively, from 5.7 to 1.5, for the oxygen treatment and from 1.5 to 0.5 for the argon and oxygen treatment.

However, for the same plasma treatment, according to figure 20, maintaining the temperature and EDA concentration, the amine groups density is higher in solutions with ethanol (W2050 and E2050 samples) than with water. Also, for the same EDA concentration and using water as solvent (W2050 and W5050 samples) the highest temperature led to the highest amino group density, which indicates that temperature may favor the reaction process improving the covalent linking between PET surface and EDA.
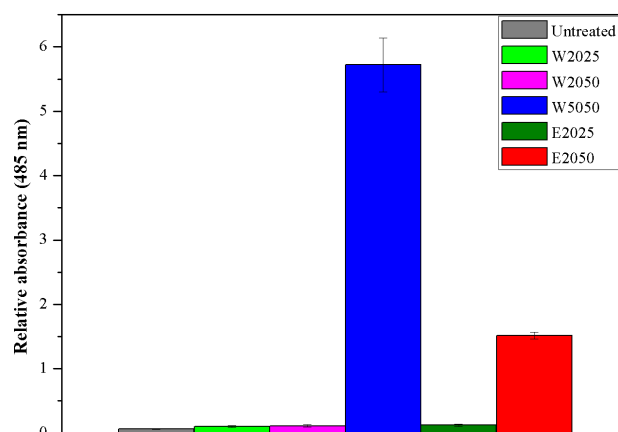
Figure 20 - Amino group density on untreated and EDA grafted samples, for 8 min oxygen plasma treatment, based on acid orange absorbance.

Since the 8 min oxygen plasma treatment results revealed to be more interesting for amino functionalization than the argon and oxygen treatment, the water contact angle, SEM and Optical profilometer analysis were only preformed on samples treated with oxygen. For this reason, since D-Lysine grafting has the

same final objective than the EDA grafting, only 8min oxygen plasma was performed.

3.4.3.3. Contact Angle

In figure 21 is possible to see the values of water contact angle for untreated PET and EDA grafting samples W5050 and E2050. In this case, it is important to measure the grafted surface contact angle in order to see if the PET surface is more hydrophilic, to allow a better cell adhesion.
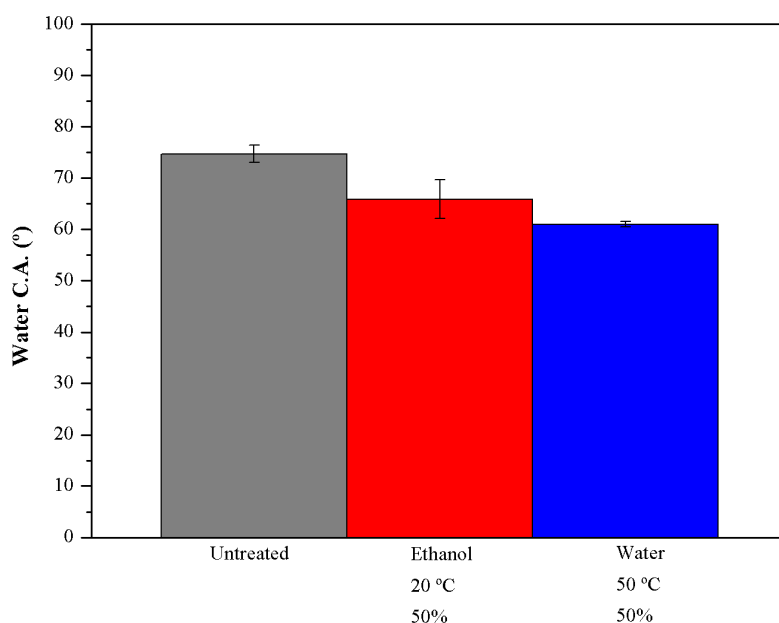
Figure 21 – Water contact angle for untreated and EDA grafted samples.

When compared with the untreated PET, both treatments result in a decrease of θ leading to more wettability, decreasing from 74.7 ° to 65.9 ° and 61.0 ° for the E2050 and W5050 samples, respectively. It has been found that when using the EDA solution, using water solvent, besides aminolysis (figure 17) other reactions like hydrolysis take place, creating more functional groups that easily react with EDA to produce $–COO^-.NH^{3+}-$, turning the PET surface more hydrophilic. On the other hand, for the EDA solution using ethanol solvent, the PET ester group on the surface can't be hydrolyzed, being the E2050 sample more hydrophobic than the one treated in water **[68, 73].**

Moreover, the contact angle is related with the amino group density because of its hydrophilic character. So, the lowest contact angle observed for the W5050

sample is in accordance with the FTIR-ATR and acid orange results (see figures 18 and 19), where more amino groups led to a surface more wettable **[66]**.

3.4.3.4. SEM analysis

SEM analysis was performed in an untreated sample (figure 22-a) and W5050 (figure 22-b) and E2050 (figure 2-c) samples, which were previously exposed to 8 min oxygen plasma treatment.

The SEM image corresponding to the untreated PET (figure 22-a) revealed an uniform surface without any relevant imperfections.

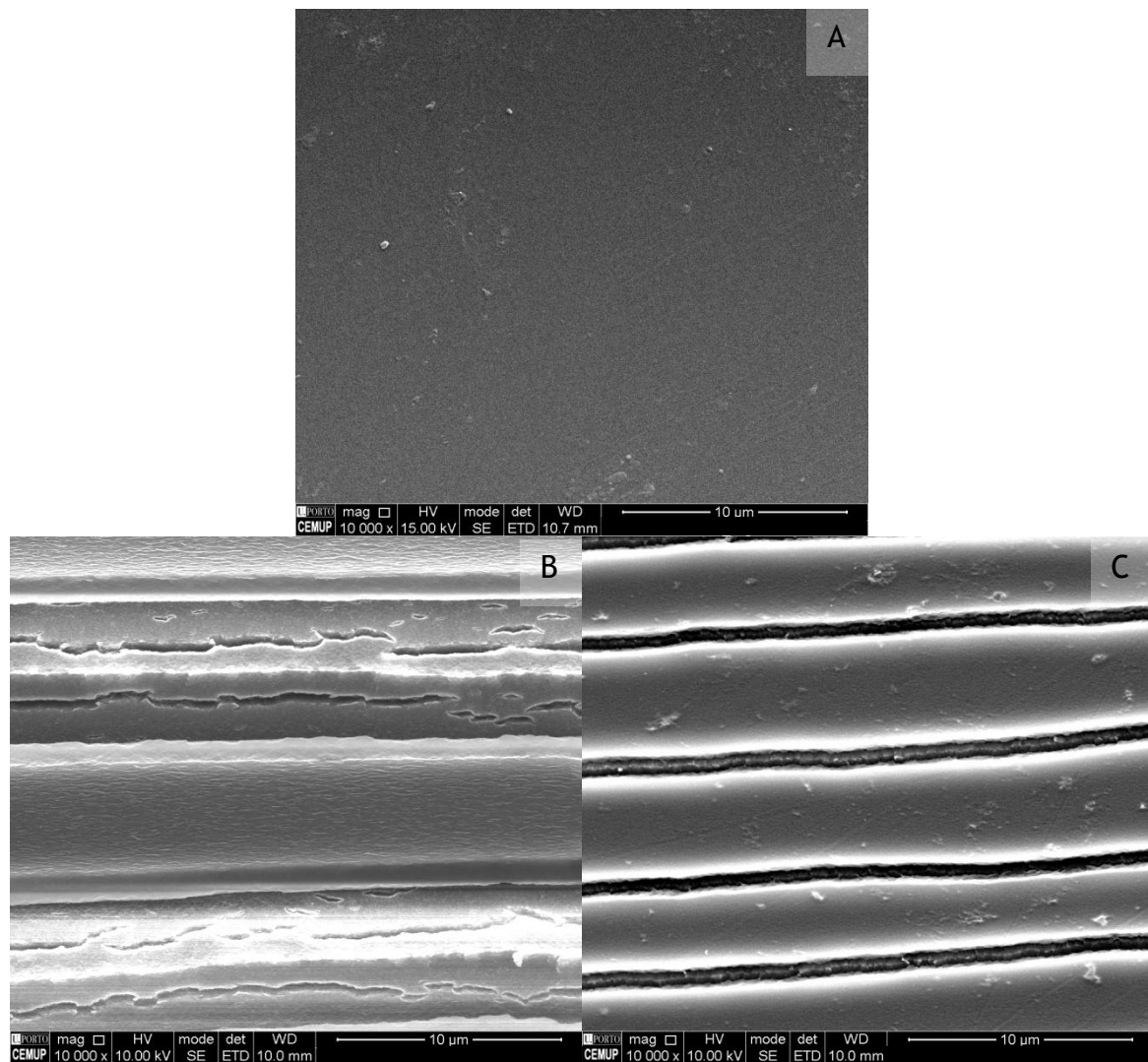**Figure 22 – SEM images of the samples surface at a magnification of 10 000x; a) untreated PET sample; b) W5050 sample; c) E2050 sample.**

The SEM images corresponding to the EDA treated samples (figure 22-b and 22-c), present aligned and parallel "strips" in the surface of the PET, in-between these oriented "strips" the space thickness is regular through the sample.
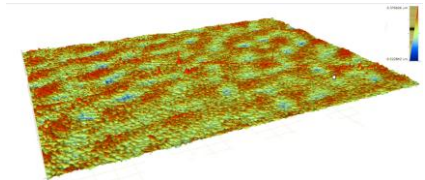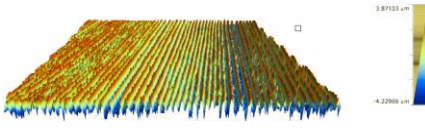
This kind of topography is explained because the EDA etches the amorphous regions between the crystallites and the polymer crystalline structure remains. Also, the alignment of the "strips" may be explained because this orientation is going to correspond to the membrane longitudinal production, since Goodfellow PET membrane is biaxial oriented **[74]**.
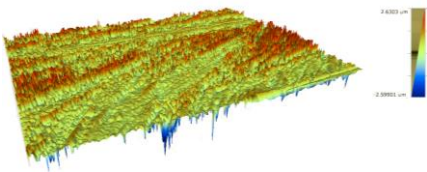
Between the W5050 and E2050 samples, the E2050 (figure 22-c) seems to have a thinner grafting because it is visible the surface original imperfections, unlike W5050 sample (figure 22-b) which seems to have a higher thickness. This indicates that the E2050 sample presents a coating with low thickness, which is in accordance with the FTIR-ATR and acid orange method results where the amino group peaks are less intense and there is also a low amino group density, respectively.

3.4.3.5. Optical Profilometer

In order to observe the surface topography and roughness after EDA grafting, the treated samples were analysed by optical profilometer in order to analyse a larger area. Table 5 shows the average roughness (R_a), standard deviation of surface heights (R_q) and a representative 3D height image for the different conditions.

Table 5 – Roughness results for the untreated PET sample and EDA grafted samples.

Treatment	Sample	R_a (nm)	R_q (nm)
Untreated		9.0 ± 1	12 ± 2
W5050		508 ± 31	612 ± 41

E2050		168 ± 66	238 ± 87

As it can be seen, both EDA treatments increase the PET surface roughness, presenting a distinct morphology, similar to the one presented on SEM images (figure 22-b and 22-c).

As it was analysed before, the W5050 sample seemed to have a higher thickness than the E2050 one. The results presented in table 5 confirm the conclusions taken from the SEM images because the W5050 sample presented a higher roughness than the E2050 sample. Moreover, when the roughness increases the surface contact area also increases and enhances the cell adhesion, this may indicate that the W5050 sample is more appropriate for cell adhesion and proliferation, due to its higher roughness and surface area **[75]**.

3.4.4. D-Lysine grafting

Since D-Lysine is the monomer of the Poly-D-Lysine, it may have a similar interaction with cell membrane when used in the adequate concentration. Also, it has the advantage of being cheaper than using directly Poly-D-Lysine.

For the D-Lysine treatments, it was study the effect of the pH in the link of D-Lysine to the PET surface. The two selected pH values (7 and 9.5) were chosen because of its effect on Lysine chemical structure (see figure 23). At pH 7, both amino groups are protonated and may both link to the carboxyl groups created on PET surface, after plasma treatment, so less amine groups would be available to interact with cells. On the other hand, at pH 9.5 this phenomenon won't happen because only one amino group is protonated to link with PET surface, being one exposed and available to interact with the living tissue **[76]**.
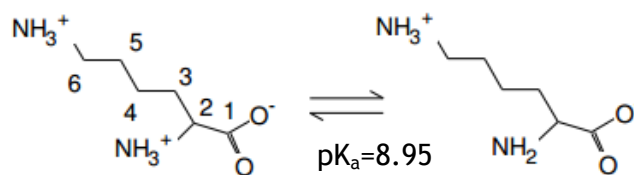
Figure 23 – Effect of pH on Lysine chemical structure [76].

3.4.4.1. FTIR-ATR

Figure 24, shows the FTIR-ATR spectra of PET, untreated and after the D-Lysine grafting with pH 7 and pH 9.5 solutions.
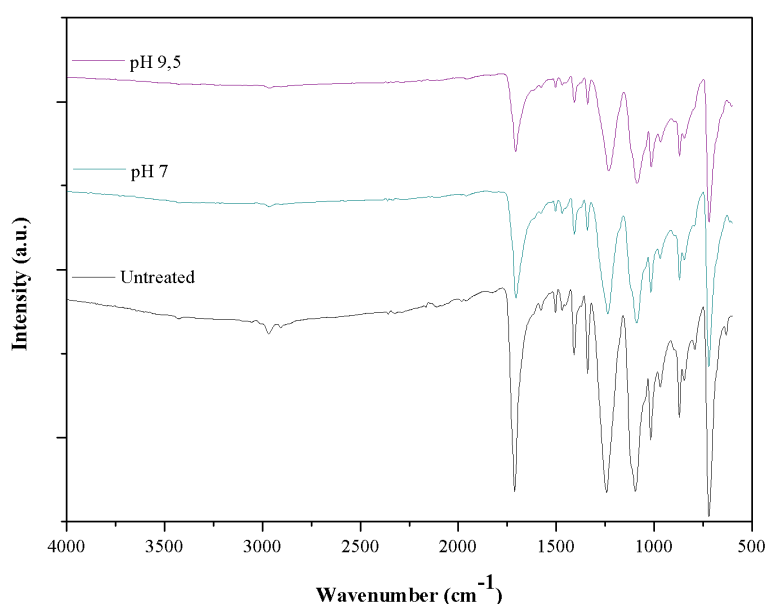
Figure 24 – FTIR-ATR spectra of untreated PET samples and D-Lysine grafted samples.

When comparing the untreated PET sample with the D-Lysine grafted samples, no new peaks were observed. Nevertheless, FTIR-ATR signal peaks are attenuated which indicates the deposition of a coating on PET surface for both pH conditions. Between the two pH conditions, the FTIR-ATR spectrum of the pH 9.5 is more attenuated, which may indicate the presence of a thicker coating, thus higher link between the D-Lysine and PET surface.

3.4.4.2. SEM analysis

SEM analysis was performed in an untreated sample (figure 25-a), D-Lysine pH 7 (figure 25-b) and D-Lysine pH 9.5 (figure 25-c) samples.

The SEM image corresponding to the untreated PET (figure 25-a) revealed an uniform surface without any relevant imperfections.
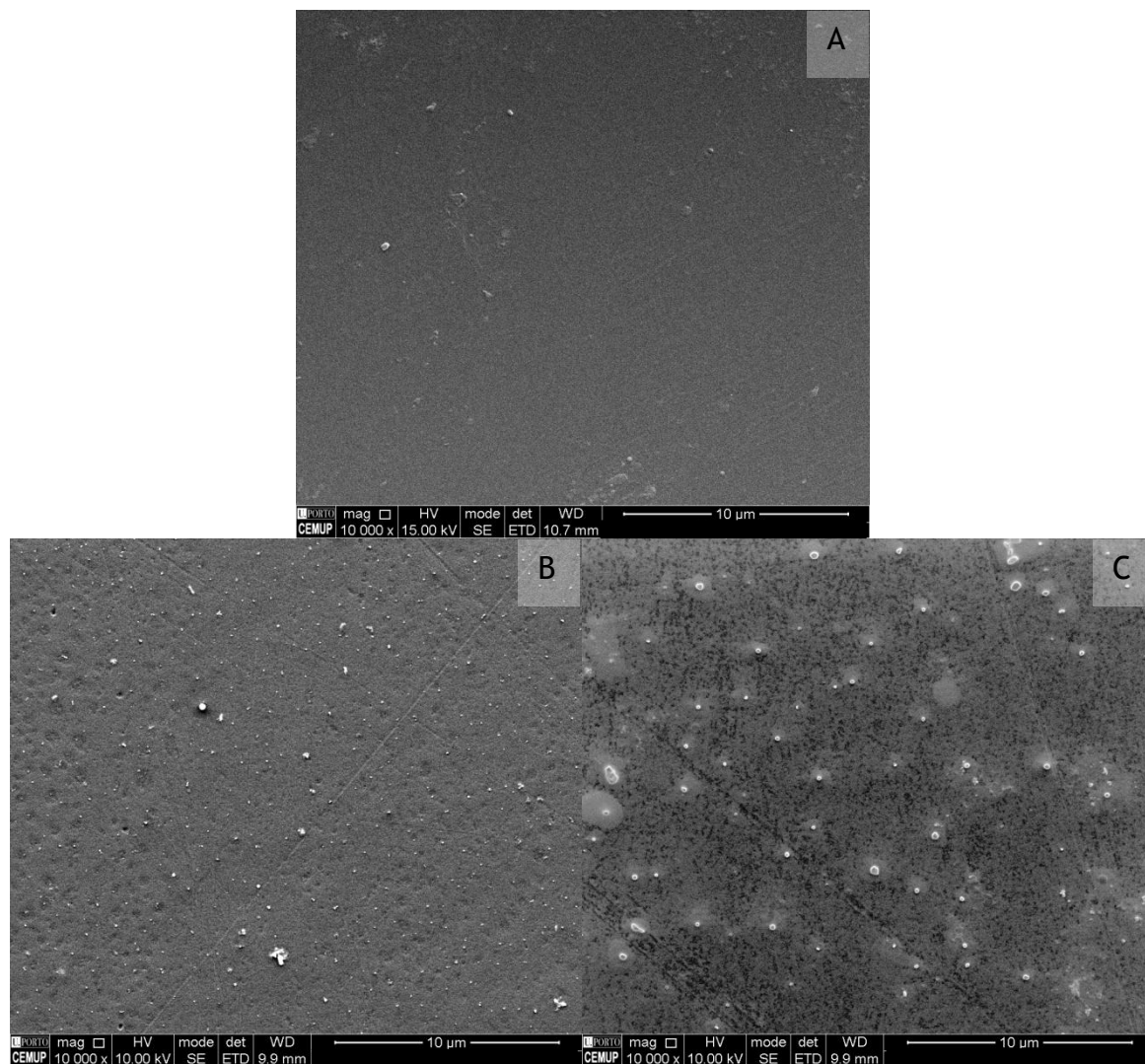
Figure 25 - SEM images of the surface samples at a magnification of 10 000x; a) untreated PET sample; b) pH 7 sample; c) pH 9.5 sample.
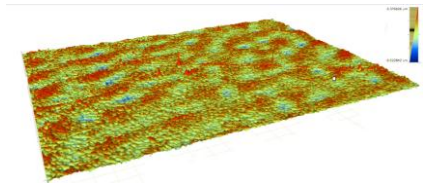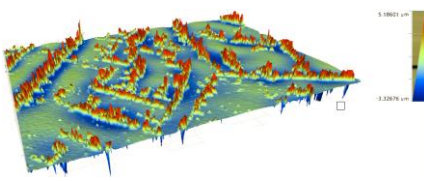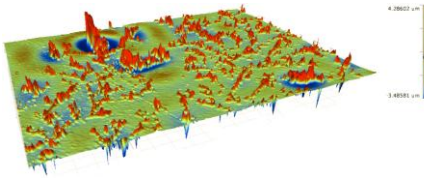
The SEM images of D-Lysine grafting (figures 25-b and 25-c) present that both conditions led to a surface coating with low thickness, since it is possible to see the original PET surface imperfections. Moreover the surface is covered with white structures that may be salt crystallized structures from the PBS solution, being difficult to distinguish it from D-Lysine. Like the FTIR-ATR results, that does not detected new amino groups peaks, the SEM images did not allow to identify the D-Lysine coating, once it is very thin and may be agglomerated on the salt structures as reported in literature **[77]** for a coating of collagen with PBS solution.

3.4.4.3. Optical Profilometer

In order to observe the surface topography and roughness after D-Lysine grafting, the treated samples were analysed by optical profilometer in order to analyse a larger area. Table 6 shows the average roughness (R_a), standard deviation

of surface heights (R_q) and a representative 3D height images for the different conditions.

Table 6 - Roughness results for the untreated PET sample and D-Lysine grafted samples.

Treatment	Sample	R_a (nm)	R_q (nm)
Untreated		9.0 ± 1	12 ± 2
pH7		149 ± 49	272 ± 81
pH 9.5		96 ± 50	183 ± 97

Similar to the EDA grafting, both D-Lysine treatments increase the PET surface roughness, presenting a distinct morphology that may be attribute to the crystal salt presence, as reported before.

Between the two D-Lysine conditions (pH 7 and pH 9.5), no big difference is observed on surfaces roughness, where the crystals salt are the main cause of surface roughness and its distribution is heterogeneous. Once more, the presence of D-Lysine cannot be distinguish from the crystal salts, as it was described for the SEM images (figure 25-b and 25-c).

3.4.4.4. Contact Angle

In figure 26 is possible to see the values of water contact angle for D-Lysine grafting using pH 7 and pH 9.5.
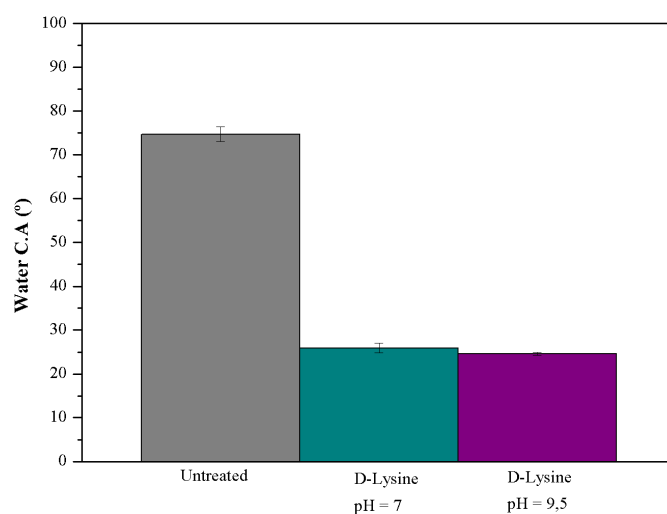
Figure 26 - Water contact angle for untreated PET sample and D-Lysine grafted samples.

Relating untreated PET sample with D-Lysine treated ones, the latter ones led to a decrease of θ, meaning a higher wettability as it was expected due to the amine group functionalization. A decrease from 74.7 ° to 25.9 ° and 24.6 ° were observed for the pH7 and pH 9.5 treatments, respectively. Between the two pH conditions, no significant difference can was detected through this evaluation, being both conditions able to increase greatly PET surface hydrophilicity.

Although the other evaluations did not allow the precise identification of D-Lysine, the significant θ decrease indicates that D-Lysine is present, otherwise the θ value would not be so low and the PET surface would not present a higher wettability.

For in vitro cell culture studies the conditions that presented to be more interesting to study were, for the EDA grafting, the W5050 condition since it presented the highest amino groups density and wettability and, for the D-Lysine grafting, the pH 9.5 condition since it FTIR-ATR spectrum were more attenuated and presented the highest wettability.

3.4.5. Cell viability evaluation

In the field of tissue engineering, focusing on repairing damaged tissue, it is required significant improvements for effective human application, being an important task the cell-material interactions control, in which the scaffold must promote cell adhesion and proliferation. In order to better understand the

influence of the surface grafting being studied (EDA and D-Lysine) on the behaviour of fibroblast cells adhesion and proliferation, these cells were cultivated *in vitro* on the different PET surface conditions (untreated and with EDA and D-Lysine grafting) and it was evaluate the cell viability using resazurin assay and SEM analysis **[77]**.

3.4.5.1. Resazurin assay

The fibroblast cells metabolic activity seeded on the untreated PET, EDA (W5050) and D-Lysine (pH 9.5) grafting on PET surface was evaluate and compared by the resazurin assay. Resazurin has been generally used as an indicator of cell viability and its reduction is correlated with the cell activity, since living cells are able to reduce the resazurin. Therefore the results presented in figure 27 are proportional to cell metabolism and therefore cell viability **[78]**.

As observed in figure 27, all the tested samples presented a metabolic activity increase with time, being the EDA grafting sample (W5050 condition) that, over time, always present more cell metabolic activity, followed by the D-lysine grafting sample (pH 9.5 condition) and untreated PET surface, that presents the lower cell metabolic activity.
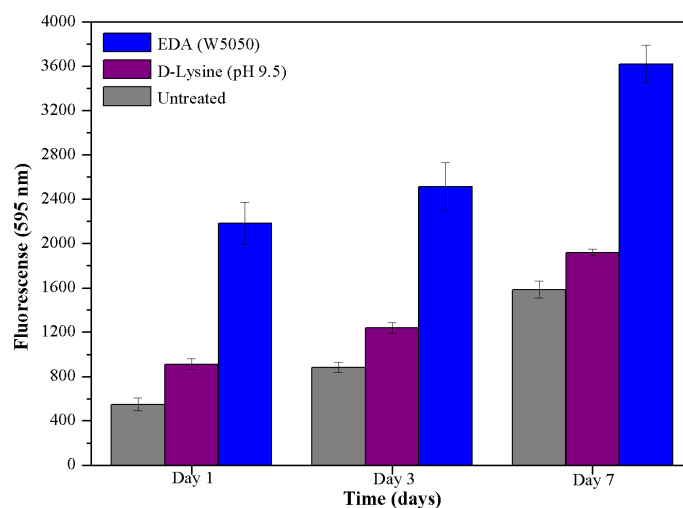

Figure 27 – Metabolic activity of L929 cells seeded on the untreated and the two developed surface grafting, after 1, 3 and 7 days of incubation.

Observing figure 27, among the tested sample the untreated PET presents the lowest cell metabolic activity because of its lack of functional groups and low wettability leading to the lowest cell adhesion and growth on its surface as

expected since these parameters are described to be important on cell-material interaction[66].

For the EDA grafting, since amine functionalization has shown to be a good mean to improve cell adhesive properties and this approach presented the highest amine concentration (see figure 18 and 19), it induced a higher cell growth than the other approach. Moreover, the EDA grafted sample surface roughness and topography (see table 5) may increase cell adhesion since it has been proved that a wavy 3D system is more cell friendly than a flat and groove surface. Therefore, the groove dimensions may have allowed cell anchorage and the alignment of cells through the orientation of the surface features may also contributed to the highest cell adhesion [79, 80].

Regarding the D-lysine grafting, the cell metabolic activity revealed that the PET surface was modified since it allowed a better cell growth than the untreated. This behaviour can be explained by the electrostatic interaction of the positively charged D-Lysine with the negative charges of the cell membrane and, also, by the high wettability of its surface that improves cell adhesion on the surface [69].

3.4.5.2. SEM analysis

Cell attachment, adhesion and spreading belong to the first phase of cell/material interaction and are very important steps for determine the performance of tissue scaffolds. The way this phenomenon occurs influences the cell growth, which is going to affect the tendon tissue regeneration. Therefore, SEM analysis was performed in order to observe cell adhesion and morphology on the different PET samples [81].

Figure 28 shows the cell growth on the untreated PET, over the 3 culture time points studied. In figure 28-a it is also possible to observe the untreated PET surface, before cell seeding.
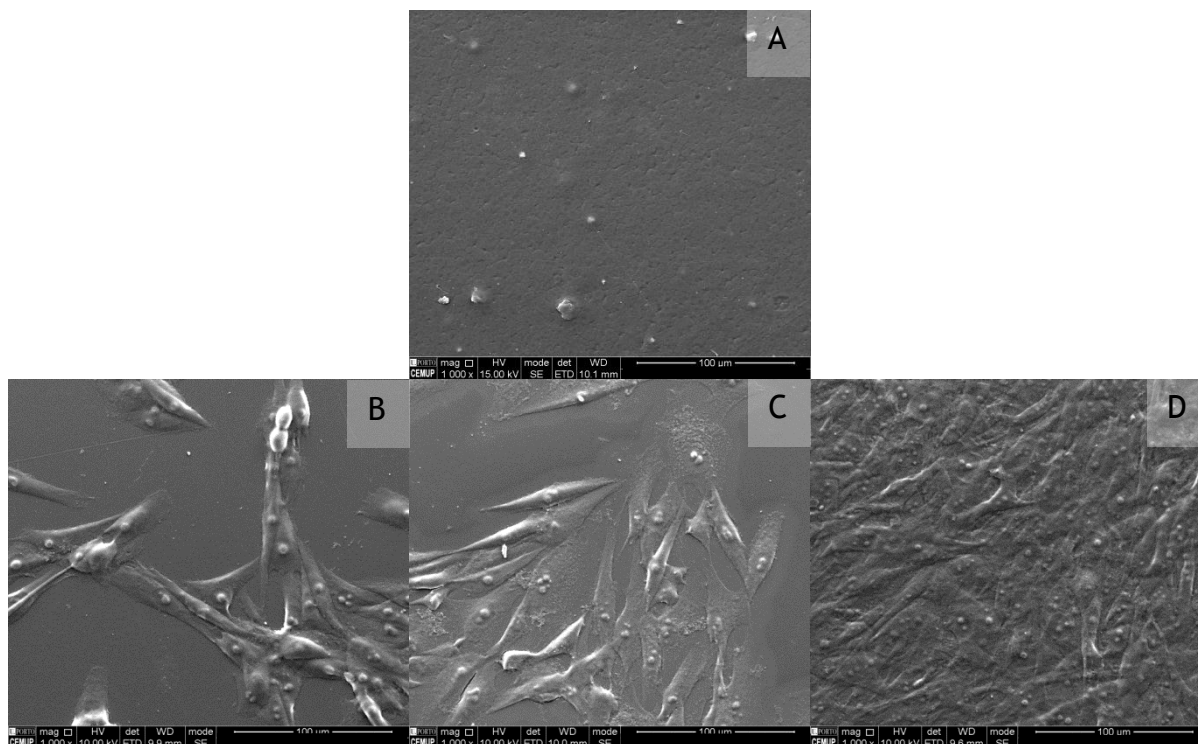
Figure 28 – SEM analysis of untreated PET samples: a) without cell seeding; b) 1 day of incubation; c) 3 days of incubation and d) 7 days of culture.

Observing figures 28-b, 28-c and 28-d it is possible to see that cell adhesion occurred and cell growth increased over culture time, even though the cells presented different morphologies In figure 28-b it can be seen that some of the seeded cells after day 1 presented a spherical shape and most of them have not started to grow, indicating the initial stage of adhesion. On the other hand, cells at day 3 and day 7 (figures 28-c and 28-d, respectively showed to be in a more advanced stage of adhesion because cells presented a more spread shape and cells growth have occurred covering the untreated PET surface gradually with culture time. These results are in accordance with the resazurin assay, where it was concluded that the cell metabolic activity increased due to cell growth.

Figure 29 shows the cell growth for the EDA grafted samples (condition W5050), over all the culture times studied. In figure 29-a it is possible to observe the PET surface morphology with the EDA grafting before cell seeding.
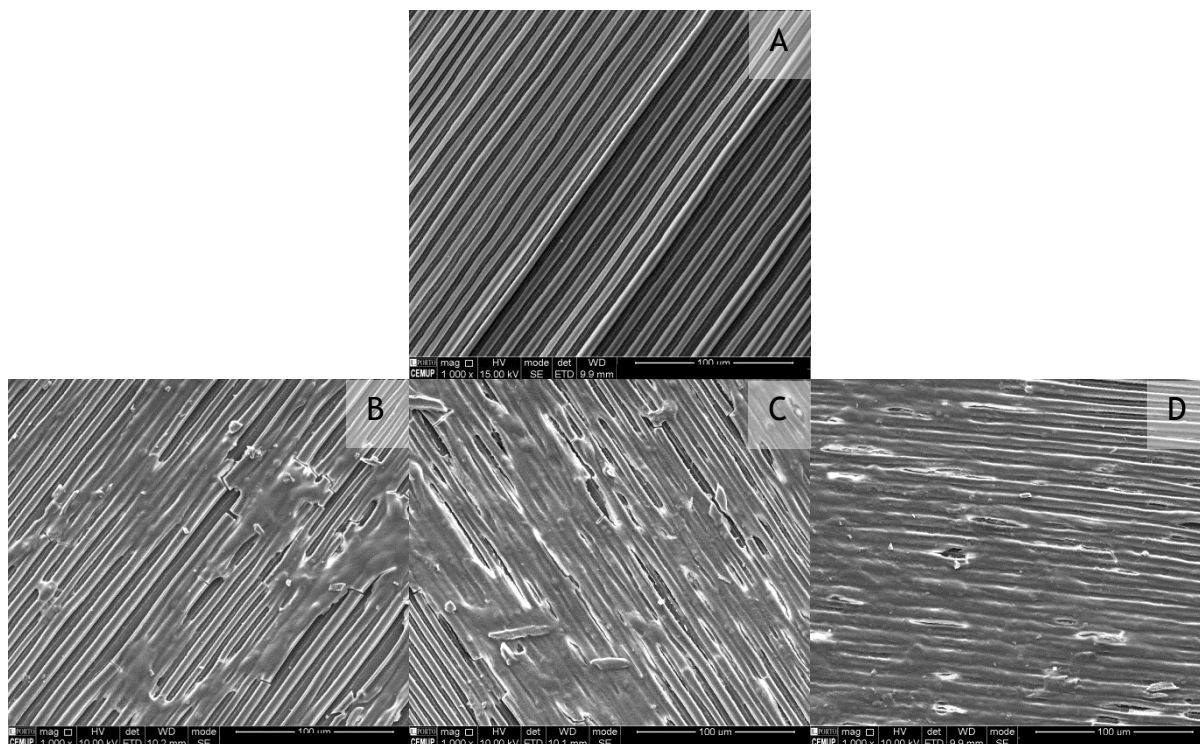
Figure 29 - SEM analysis of EDA grafted (W5050) PET samples: a) without cell seeding; b) 1 day of incubation; c) 3 days of incubation and d) 7 days of culture.

Observing figures 29-b, 29-c and 29-d it is possible to see that, like the resazurin assay results showed, cell adhesion occurred and cell growth increased over culture time. For all culture times, cells presented a well spread shape, being oriented with the grafted structure. Although after day 1 and day 3 it is still possible to see the original surface morphology, at day 7 the cells have grown and spread all over the surface forming a continuous cell layer.

Although at day 1 and day 3 (figure 29-b and 29-c, respectively) the samples surface did not seem to be completely covered by the cells, optical microscope observation indicated that cell growth and distribution occurred through the surface since day 1. Figure 30 shows the optical microscope images, in which cells were coloured, for the EDA grafted PET surface at the different culture time points studied.
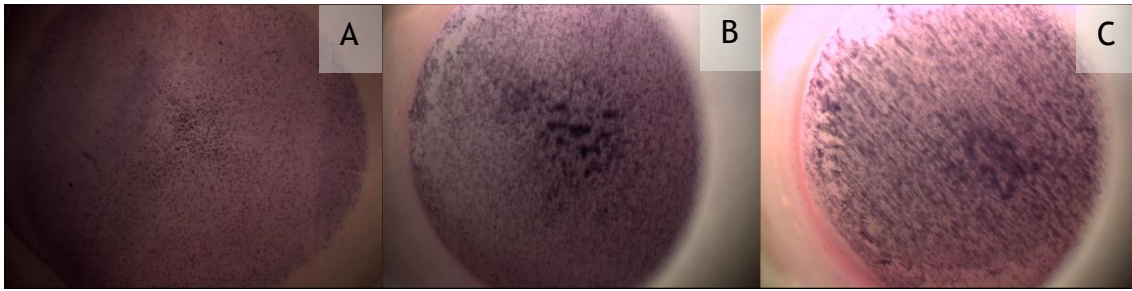
Figure 30 – Optical microscope images for EDA grafted samples: a) 1 day incubation; b) 3 day incubation and c) 7 day incubation.

Figure 30 images are in accordance with the resazurin results, where the longest cell culture time led to the highest cells density, which covered completely the sample surface. These results show that SEM images did not represent the real cell growth distribution that have occurred and it may be a result of cell detachment from the surface during have the cell fixation and dehydration steps needed for SEM analysis, due to the high cells number grown on these samples.

Lastly, Figure 31 shows the cell growth for the D-Lysine grafted samples (condition pH 9.5), over the 3 time points studied. In figure 31-a it is possible to observe the PET surface morphology with the D-Lysine grafting, where less crystal salts were presented, when compared with figure 25-c, indicating that they don't cover all surface.
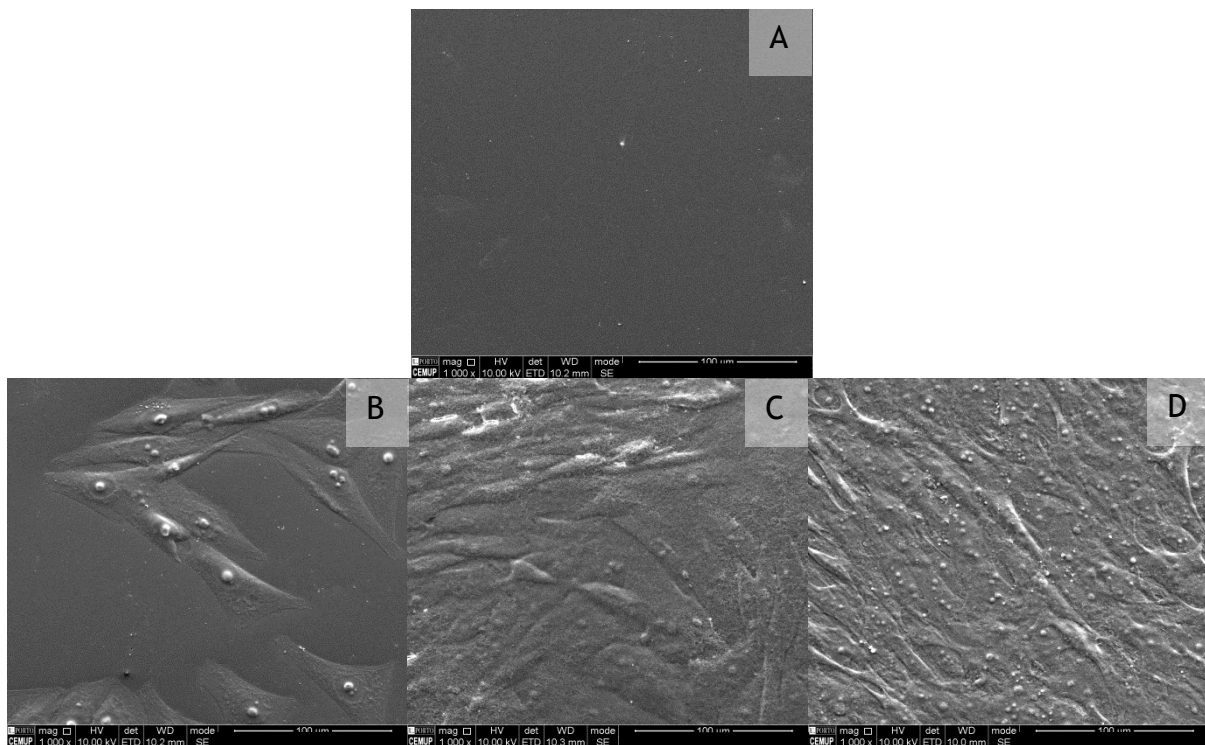
Figure 31 – SEM analysis of D-Lysine grafted (pH 9.5) PET samples: a) without cell seeding; b) 1 day of incubation; c) 3 days of incubation and d) 7 days of culture.

Once again, observing figures 31-b, 31-c and 31-d it is possible to see that, cell adhesion occurred and cell growth increased over culture time since the sample surface could be seen at day 1 but at day 7 it is not exposed. The SEM images are in accordance with the resazurin results. For all incubation times, cells presented a well spread shape, but at days 3 and 7 the cells are not so well defined, indicating that some residues from the cell culture preparation may be presented.

The spread shape of cells observed in SEM images are formed due to the organization of the cytoskeleton filamentous proteins, which tend to assemble in long bundles, leading to this kind of morphology, named filopodia, of the plasma membrane. The cytoskeleton organization will, as consequence, control the cell morphology and, once cell adhesion is establish, the cell shape can also be related with the cell growth **[81, 82].**

CONCLUSIONS

Nowadays tendon injuries are frequent and affect not only the older population but also younger people, once they are many times associated with the practice of sports and lifestyle.

Although there are some scaffolds available in the market, the future treatments aim to use functional scaffolds that help the new tendon tissue to closely mimic the native tendon. For that, the scaffold design must be similar to the tendon hierarchal structure and its materials shall allowed a better cell-surface interaction, such as cell adhesion, proliferation and differentiation and tissue ingrowth.

In chapter 2, PET textile structures developed by Diana Morais were characterized at the physical, chemical and mechanical level. For the single PET yarn, DSC and XRD demonstrated both a crystallinity degree of 55%, the weight change during swelling and the capillary rise during the vertical wicking test revealed water absorption, the yarn presented lower mechanical properties than the braided structures, and no degradation occurred during the time points tested.

Regarding the braided structures, the one that presented to be more suitable for a future application in the scaffold being developed by Diana Morais is the braid with 16 yarns made at a high take-up rate (16YH) because its design (number of fibers and braid angle) allowed this structure to present the best performance of capillary rise and mechanical properties level when compared with the other braided structures.

In chapter 3, in order to functionalize the PET surface it was perform initially an oxygen plasma treatment to increase the PET hydrophilicity. After plasma treatment, two grafting approaches were performed, with EDA and D-Lysine.

For the EDA grafting, FTIR-ATR and acid orange results allowed to choose the conditions with the best amino functionalization, which were W5050 and E2050. Other techniques, such as water contact angle measurement, SEM analysis and optical profilometry indicated that, between the W5050 and E2050 treatments, the W5050 would be the one more suitable to enhance cell adhesion, since it presented

the highest amino groups, the lowest water contact angle and the highest grafting thickness and roughness.

Regarding the D-Lysine grafting, two pH solutions were tested (pH 7 and 9.5). The same steps were performed to choose the best condition to promote cell adhesion. Although FTIR-ATR didn't show the presence of amino groups, the attenuation of the peaks, when comparing with the untreated PET sample, indicated that grafting may have occurred and between the two pH conditions the pH 9.5 condition properties revealed to be more interesting for cell culture studies. Moreover the decrease of the water contact angle indicated that D-Lysine grafting may have been successful.

Once the best grafting conditions were chosen, the aim of this work was also to study the cellular response to the developed PET surface functionalization. Thus, resazurin and SEM analysis were performed in order to analyse cell adhesion, proliferation and morphology. The EDA grafting (W5050 condition) was the approach that showed the best results, since it demonstrate higher cell metabolic than the untreated and D-Lysine grafted samples, through all the culture time indicating cell proliferation. Moreover, SEM results corroborate this conclusion, since cell were spread through the surface indicating a good adhesion and cell growth occurred being the surface all covered by cells at day 7. Nevertheless, D-Lysine grafted samples also presented better cell response than PET untreated sample indicating that the grafting occurred and it is suitable for surface functionalization aiming cell adhesion and proliferation.

In conclusion, both grafting approaches enhanced the untreated PET surface properties, such as surface hydrophilicity and cell adhesion and proliferation, indicating that these grafting methods may be applied on the tendon scaffold.

FUTURE WORK

With the aim of continue this study on tendon scaffold application, the next step would be to apply these grafting methods on PET yarn being used on the scaffolds under development, and study the effect of surface modification on PET yarn on physico-chemical and mechanical properties and cellular response. If successful, the functionalization could be applied on the braided structure of the optimized scaffold. Once all the parameters are optimized, further *in vivo* tests must be performed with the objective to evaluate the animal biological response.

REFERENCES

1. Rodrigues, M.T., R.L. Reis, and M.E. Gomes, *Engineering tendon and ligament tissues: present developments towards successful clinical products*. Journal of Tissue Engineering and Regenerative Medicine, 2013. **7**(9): p. 673-686.
2. Longo, U.G., et al., *Scaffolds in tendon tissue engineering*. Stem Cells Int, 2012. p. 1-8.
3. Awad, H., *Prospects of tendon tissue engineering in sports medicine*. Deutsche Zeitschrift fur Sportmedizin, 2012. **63**(5): p. 132.
4. Maffulli, N., P. Renström, and W.B. Leadbetter, *Tendon injuries : basic science and clinical medicine*. 2005, London: Springer.
5. Chen, J., et al., *Scaffolds for tendon and ligament repair: review of the efficacy of commercial products*. Expert Review of Medical Devices, 2009. **6**(1): p. 61-73.
6. Sharma, P. and N. Maffulli, *Biology of tendon injury: healing, modeling and remodeling*. J Musculoskelet Neuronal Interact, 2006. **6**(2): p. 181-90.
7. Hoffmann, A. and G. Gross, *Tendon and ligament engineering: from cell biology to in vivo application*. Regen Med, 2006. **1**(4): p. 563-74.
8. Johnson, K.E. and K.E. Johnson, *Histology and cell biology*. 1991, USA: Williams & Wilkins.
9. Wang, J.H., *Mechanobiology of tendon*. J Biomech, 2006. **39**(9): p. 1563-82.
10. Hampson, K., et al., *Tendon tissue engineering*. Topics in tissue engineering, 2008. **4**.
11. Kannus, P., *Structure of the tendon connective tissue*. Scand J Med Sci Sports, 2000. **10**(6): p. 312-20.
12. Sharma, P. and N. Maffulli, *Tendon Injury and Tendinopathy: Healing and Repair*. Vol. 87. 2005. 187-202.
13. Jung, H.J., M.B. Fisher, and S.L. Woo, *Role of biomechanics in the understanding of normal, injured, and healing ligaments and tendons*. Sports Med Arthrosc Rehabil Ther Technol, 2009. **1**(1): p. 9.
14. James, R., et al., *Tendon: Biology, Biomechanics, Repair, Growth Factors, and Evolving Treatment Options*. Journal of Hand Surgery, 2008. **33**(1): p. 102-112.
15. Kuo, C., J. Marturano, and R. Tuan, *Novel strategies in tendon and ligament tissue engineering: Advanced biomaterials and regeneration motifs*. Sports Medicine, Arthroscopy, Rehabilitation, Therapy & Technology, 2010. **2**(1): p. 1-14.
16. Bass, E., *Tendinopathy: Why the Difference Between Tendinitis and Tendinosis Matters*. International Journal of Therapeutic Massage & Bodywork, 2012. **5**(1): p. 14-17.
17. Wren, T.A., et al., *Mechanical properties of the human achilles tendon*. Clin Biomech (Bristol, Avon), 2001. **16**(3): p. 245-51.
18. Shearn, J.T., et al., *Tendon tissue engineering: progress, challenges, and translation to the clinic*. J Musculoskelet Neuronal Interact, 2011. **11**(2): p. 163-73.

19. Lin, T.W., L. Cardenas, and L.J. Soslowsky, *Biomechanics of tendon injury and repair*. J Biomech, 2004. **37**(6): p. 865-77.
20. Liu, Y., H.S. Ramanath, and D.A. Wang, *Tendon tissue engineering using scaffold enhancing strategies*. Trends Biotechnol, 2008. **26**(4): p. 201-9.
21. Bagnaninchi, P.O., et al., *Tissue engineering for tendon repair*. Br J Sports Med, 2007. **41**(8): p. 1-5.
22. Moshiri, A. and A. Oryan, *Role of tissue engineering in tendon reconstructive surgery and regenerative medicine: current concepts, approaches and concerns*. Hard Tissue, 2012. **1**(2): p. 11.
23. Bassetto, F., A. Volpin, and V. Vindigni, *Regenerative Medicine for Tendon Regeneration and Repair: The Role of Bioscaffolds and Mechanical Loading*. 2011. Italy:InTech. p.370-86.
24. Reverchon, E., et al., *Biodegradable synthetic scaffolds for tendon regeneration*. Muscles, Ligaments and Tendons Journal, 2012. **2**(3): p. 181-186.
25. James, R., *Novel Tissue Engineering Strategies for Tendon Repair and Regeneration*. 2012: University of Virginia.
26. Longo, U.G., et al., *Tendon augmentation grafts: a systematic review*. British Medical Bulletin, 2010. **94**. p.165-88.
27. Turner, N.J. and S.F. Badylak, *Biologic scaffolds for musculotendinous tissue repair*. Eur Cell Mater, 2013. **25**: p. 130-43.
28. Barber, J.G., et al., *Braided nanofibrous scaffold for tendon and ligament tissue engineering*. Tissue Eng Part A, 2013. **19**(11-12): p. 1265-74.
29. Gunatillake, P.A. and R. Adhikari, *Biodegradable synthetic polymers for tissue engineering*. Eur Cell Mater, 2003. **5**: p. 1-16; discussion 16.
30. Sahoo, S., et al., *Bioactive nanofibers for fibroblastic differentiation of mesenchymal precursor cells for ligament/tendon tissue engineering applications*. Differentiation, 2010. **79**(2): p. 102-110.
31. Sahoo, S., et al., *Characterization of a novel polymeric scaffold for potential application in tendon/ligament tissue engineering*. Tissue engineering, 2006. **12**(1): p. 91-99.
32. Chen, G., T. Ushida, and T. Tateishi, *Scaffold design for tissue engineering*. Macromolecular Bioscience, 2002. **2**(2): p. 67-77.
33. Jiang, J., et al., *Biocompatibility evaluation of polyethylene terephthalate artificial ligament coating hydroxyapatite by fibroblasts cells in vitro*. Journal of Shanghai Jiaotong University (Science), 2012. **17**(6): p. 717-722.
34. Ramachandran, M., *Basic Orthopaedic Sciences: The Stanmore Guide*. 2006: Taylor & Francis.
35. Omeroglu, S., *The effect of braiding parameters on the mechanical properties of braided ropes*. Fibres and Textiles in Eastern Europe, 2006. **14**(4): p. 53.
36. *CES EduPack*, Granta Design Limited. 2014, Cambridge: UK.
37. Sichina, W., *DSC as problem solving tool: measurement of percent crystallinity of thermoplastics*. Thermal Analysis Application Note, 2000.
38. Haji, A. and R. Semnani Rahbar, *Crystallinity and orientation development upon hot multistage drawing of PET multifilament yarn*. The Journal of The Textile Institute, 2012. **104**(3): p. 231-238.
39. Sarasua, J.R., et al., *Crystallinity assessment and in vitro cytotoxicity of polylactide scaffolds for biomedical applications*. Journal of Materials Science: Materials in Medicine, 2011. **22**(11): p. 2513-2523.

40.   Mark, J.E., *Polymer Data Handbook*. 1999: Oxford University Press.
41.   Raghavendra R. Hegde, M.G.K., Atul Dahiya. *Polymer crystallinity*. 2004; Available from: http://web.utk.edu/~mse/Textiles/Polymer%20Crystallinity.htm.
42.   Steinmann, W., et al., *Thermal Analysis of Phase Transitions and Crystallization in Polymeric Fibers*. Applications of Calorimetry in a Wide Context - Differential Scanning Calorimetry, Isothermal Titration Calorimetry and Microcalorimetry. 2013.
43.   Huang, Z., et al., *Effects of dimethylolpropionic acid modification on the characteristics of polyethylene terephthalate fibers*. Molecular medicine reports, 2012. **6**(4): p. 709-715.
44.   Nunes, R.A.X., et al., *Wear, friction, and microhardness of a thermal sprayed PET: poly (ethylene terephthalate) coating*. Materials Research, 2009. **12**: p. 121-125.
45.   Vlachou, M., et al., *Polymers for Use in Controlled Release Systems: The Effect of Surfactants on their Swelling Properties*. Journal of Biomaterials Applications, 2000. **15**(1): p. 65-77.
46.   Akinli-Kogak, S., *The influence of fiber swelling on paper wetting*. 2001, The University of Maine.
47.   Adanur, S., *Wellington Sears Handbook of Industrial Textiles*. 1995: Taylor & Francis.
48.   De, S.K., et al., *Equilibrium swelling and kinetics of pH-responsive hydrogels: models, experiments, and simulations*. Microelectromechanical Systems, Journal of, 2002. **11**(5): p. 544-555.
49.   Cooper, J.A., et al., *Fiber-based tissue-engineered scaffold for ligament replacement: design considerations and in vitro evaluation*. Biomaterials, 2005. **26**(13): p. 1523-1532.
50.   Laurencin, C.T. and J.W. Freeman, *Ligament tissue engineering: An evolutionary materials science approach*. Biomaterials, 2005. **26**(36): p. 7530-7536.
51.   Bicking, A.M. and W. Oxenham, *Variables and Methods for Aesthetic Braid Design*. Journal of Textile and Apparel, Technology and Management, 2012. **7**(4).
52.   Mardina, Z., et al. *The Influence of Braiding Angle Variation in Braided-Twisted Fiber Scaffold Based Poly L-Lactic Acid for Anterior Cruciate Ligament Reconstruction Application*. in *Advanced Materials Research*. 2014. Trans Tech Publ.
53.   Planck, H., et al., *Medical textiles for implantation*. 1990: Springer-Verlag.
54.   Tabbaa, S. and K.J.L. Burg, *The effect of wicking fibres in tissue-engineered bone scaffolds*. Journal of Tissue Engineering and Regenerative Medicine, 2015. **9**(4): p. 469-472.
55.   Oh, D.S., et al., *Effect of capillary action on bone regeneration in micro-channeled ceramic scaffolds*. Ceramics International, 2014. **40**(7, Part A): p. 9583-9589.
56.   Tabbaa, S., A. Mlynarczyk, and K.J. Burg, *Improved Cellular Recruitment and Mass Transport for Large Bone Defect Regeneration*.
57.   Hossain, M.M., et al., *Contact angle determination on plasma-treated poly(ethylene terephthalate) fabrics and foils*. Journal of Applied Polymer Science, 2006. **102**(2): p. 1452-1458.

58.   Saricam, C. and F. Kalaoglu, *Investigation of the Wicking and Drying Behaviour of Polyester Woven Fabrics.* Fibres & Textiles in Eastern Europe, 2014. **22**(3): p. 73-78.

59.   Fangueiro, R., et al., *Wicking behavior and drying capability of functional knitted fabrics.* Textile Research Journal, 2010. **80**(15): p. 1522-1530.

60.   Del Rosso, S., L. Iannucci, and P.T. Curtis, *Experimental investigation of the mechanical properties of dry microbraids and microbraid reinforced polymer composites.* Composite Structures, 2015. **125**(0): p. 509-519.

61.   Proske, U. and D.L. Morgan, *Tendon stiffness: Methods of measurement and significance for the control of movement. A review.* Journal of Biomechanics. **20**(1): p. 75-82.

62.   Turki, S., S. Marzougui, and S. Ben Abdessalem, *Impact of polyurethane yarns on the mechanical properties of braided artificial ligaments.* The Journal of The Textile Institute, 2014. **106**(9): p. 912-918.

63.   Gomes, M.E., et al., *Alternative tissue engineering scaffolds based on starch: processing methodologies, morphology, degradation and mechanical properties.* Materials Science and Engineering: C, 2002. **20**(1–2): p. 19-26.

64.   Chen, H., et al., *Fabrication of nanofibrous scaffolds for tissue engineering applications*, in *Nanomaterials in tissue engineering: Fabrication and applications*, A.K. Gaharwar, et al., Editors. 2013, Woodhead Publishing. p. 158-182.

65.   Vesel, A. and M. Mozetic. *Surface functionalization of organic materials by weakly ionized highly dissociated oxygen plasma.* in *Journal of Physics: conference series.* 2009. IOP Publishing.

66.   Hamerli, P., et al., *Surface properties of and cell adhesion onto allylamine-plasma-coated polyethylenterephtalat membranes.* Biomaterials, 2003. **24**(22): p. 3989-3999.

67.   Keen, I., et al., *Introducing Amine Functionalities on a Poly(3-hydroxybutyrate-co-3-hydroxyvalerate) Surface: Comparing the Use of Ammonia Plasma Treatment and Ethylenediamine Aminolysis.* Biomacromolecules, 2006. **7**(2): p. 427-434.

68.   Xue, L., Q. liang, and Y. Lu, *Electroless copper plating on 1,2-ethylenediamine grafted poly(ethyleneterepthalate) for the fabrication of flexible copper clad laminate.* Journal of Materials Science: Materials in Electronics, 2013. **24**(7): p. 2211-2217.

69.   Harnett, E.M., J. Alderman, and T. Wood, *The surface energy of various biomaterials coated with adhesion molecules used in cell culture.* Colloids and Surfaces B: Biointerfaces, 2007. **55**(1): p. 90-97.

70.   Sparavigna, A., *Plasma treatment advantages for textiles.* 2008. Italy: Torino

71.   Chu, P.K., et al., *Plasma-surface modification of biomaterials.* Materials Science and Engineering: R: Reports, 2002. **36**(5–6): p. 143-206.

72.   Leroux, F., et al., *Atmospheric air plasma treatment of polyester textile materials. Textile structure influence on surface oxidation and silicon resin adhesion.* Surface and Coatings Technology, 2009. **203**(20–21): p. 3178-3183.

73.   Irena, G., B. Jolanta, and Z. Karolina, *Chemical modification of poly(ethylene terephthalate) and immobilization of the selected enzymes on the modified film.* Applied Surface Science, 2009. **255**(19): p. 8293-8298.

74. Aflori, M., et al., *Amine functionality of poly (ethylene terepthalate) films surfaces induced by chemical and RF plasma treatments.*2007. Czech Republic: Prague.

75. Bessada, R., et al., *Functionalization of PET and PA6.6 woven fabrics.* Applied Surface Science, 2011. **257**(18): p. 7944-7951.

76. Nolting, D., et al., *pH-Induced Protonation of Lysine in Aqueous Solution Causes Chemical Shifts in X-ray Photoelectron Spectroscopy.* Journal of the American Chemical Society, 2007. **129**(45): p. 14068-14073.

77. Aflori, M., et al., *Collagen immobilization on polyethylene terephthalate surface after helium plasma treatment.* Materials Science and Engineering: B, 2013. **178**(19): p. 1303-1310.

78. O'Brien, J., et al., *Investigation of the Alamar Blue (resazurin) fluorescent dye for the assessment of mammalian cell cytotoxicity.* European Journal of Biochemistry, 2000. **267**(17): p. 5421-5426.

79. Allion, A., J.-P. Baron, and L. Boulange-Petermann, *Impact of surface energy and roughness on cell distribution and viability.* Biofouling, 2006. **22**(5): p. 269-278.

80. Hu, J., et al., *Enhanced Cell Adhesion and Alignment on Micro-Wavy Patterned Surfaces.* PLoS ONE, 2014. **9**(8): p. e104502.

81. Anselme, K., *Osteoblast adhesion on biomaterials.* Biomaterials, 2000. **21**(7): p. 667-681.

82. Gwynn, I., *Cell biology at interfaces.* Journal of Materials Science: Materials in Medicine, 1994. **5**(6-7): p. 357-360.
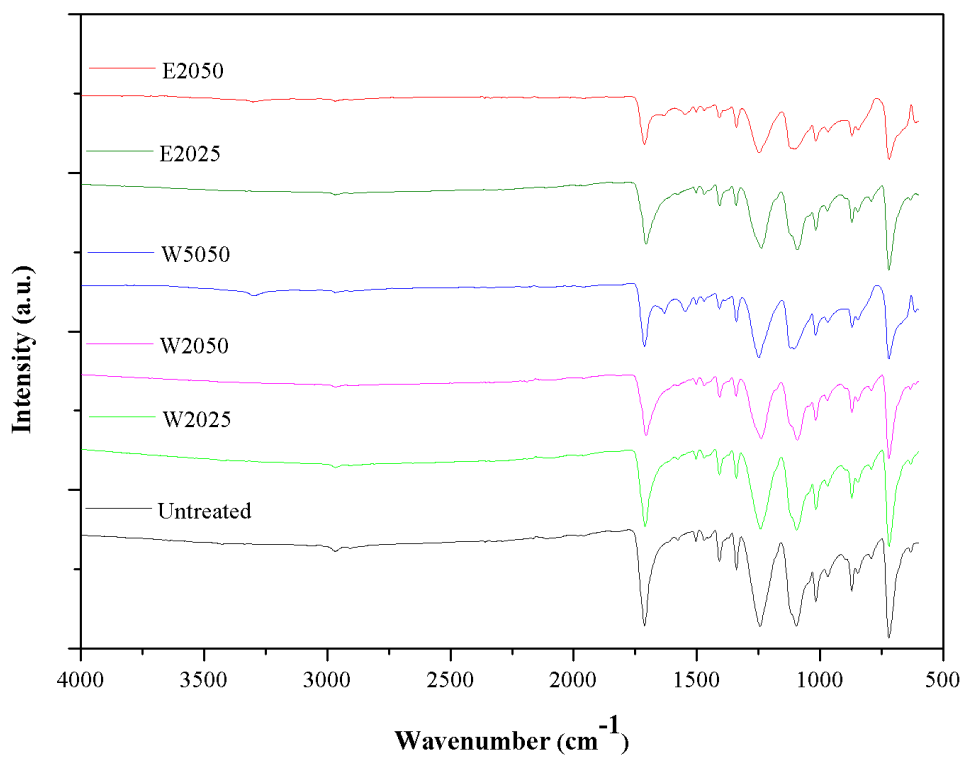
ATTACHMENTS

Figure 32 – FTIR-ATR spectra of untreated PET and EDA grafted samples, activated with 8 min oxygen plasma treatment